

Instruments for High-Energy Astrophysics (part III)

X-ray telescopes

partly adapted from G. Malaguti's and A. Bulgarelli's presentations

Telescopes for X-ray and γ -ray astronomy

Low energies ($E \leq 20$ keV)

- Proportional counters (mostly adopted in the past, 'evolution' of Geiger counters)
- Micro-channel plates (MCP; provide very good imaging; ex: *Chandra*)
- Micro-calorimeters (for high spectral resolution; ex: forthcoming *XRISM*, *Athena*)
- CCDs (widely used, valid for both imaging and moderate-quality spectroscopy, low background; ex: *Chandra*, *XMM-Newton*)

Intermediate energies ($E \approx 15$ keV – MeV)

- Scintillators (high efficiency, moderate spectral resolution)
- Solid-state detectors (high efficiency, good spectral resolution, cooling problem; ex: *NuSTAR*)

High energies ($E \approx$ MeV – GeV)


- Spark chambers and converters/trackers (ex: *Fermi*, *AGILE*)

Telescopes for X-ray and γ -ray astronomy



GRAZING INCIDENCE

(typically, $E \leq 10$ keV, with the exception of *NuSTAR*, up to ≈ 80 keV), Wolter I configuration

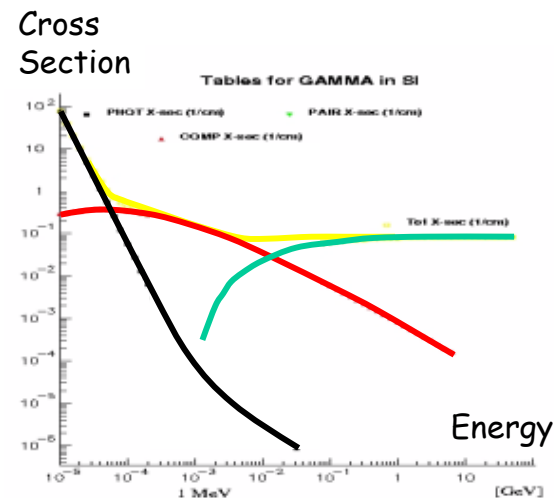
- 
- **$E \approx 20$ -100 keV:** collimators (several types), coded masks
 - **$E \approx 0.2$ -10 MeV:** Compton Telescopes
 - **$E > 10$ MeV:** Pair-production Telescopes (converters/ Spark-tracking chambers, already discussed)

Telescopes vs. Observing energy

Telescope-detector coupling

The *cross-section* of radiation-matter interaction mechanism is the key

Detection of Gamma Radiation



Photoeffect (< 100 keV)

Photons effectively blocked and stopped

Telescopes:

Collimators
Coded Mask Systems

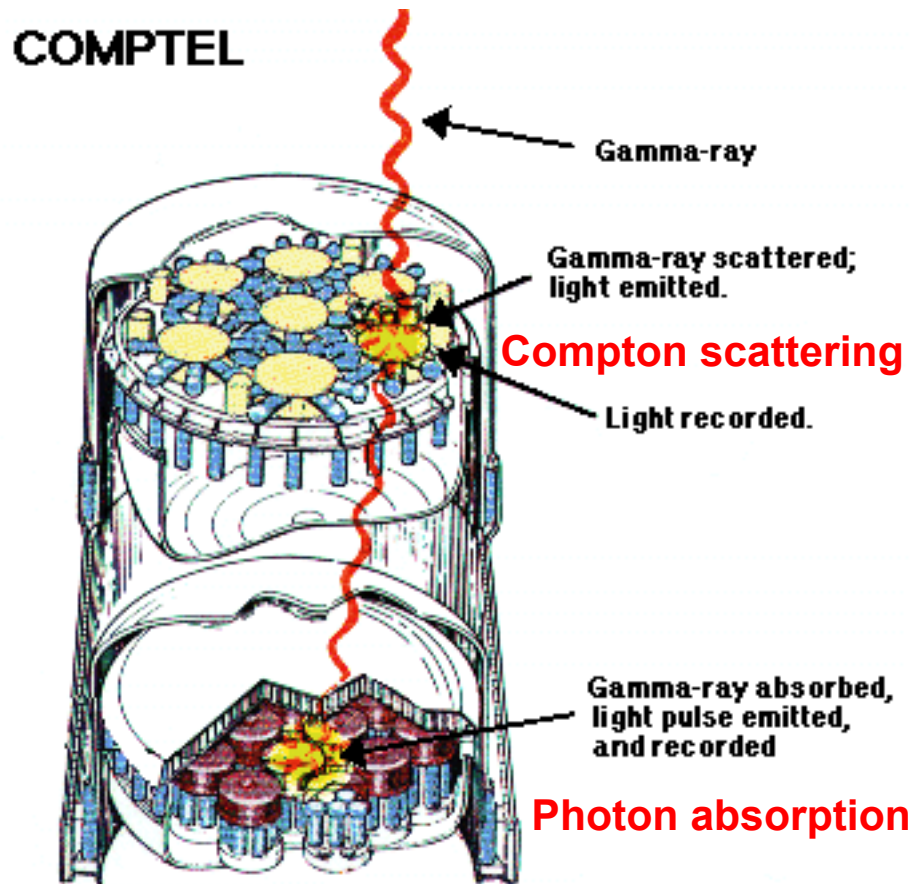
Pair Creation (> 10 MeV)
Photons completely converted to e^+e^-

Telescope:
Tracking chambers to visualize the pairs

Compton Scattering (0.2-10 MeV)
Photon Crosssection Minimum
Scattered photons with long range
Telescope:
Compton Camera Coincidence System

Compton telescopes

The Compton telescopes: COMPTEL onboard CGRO. I



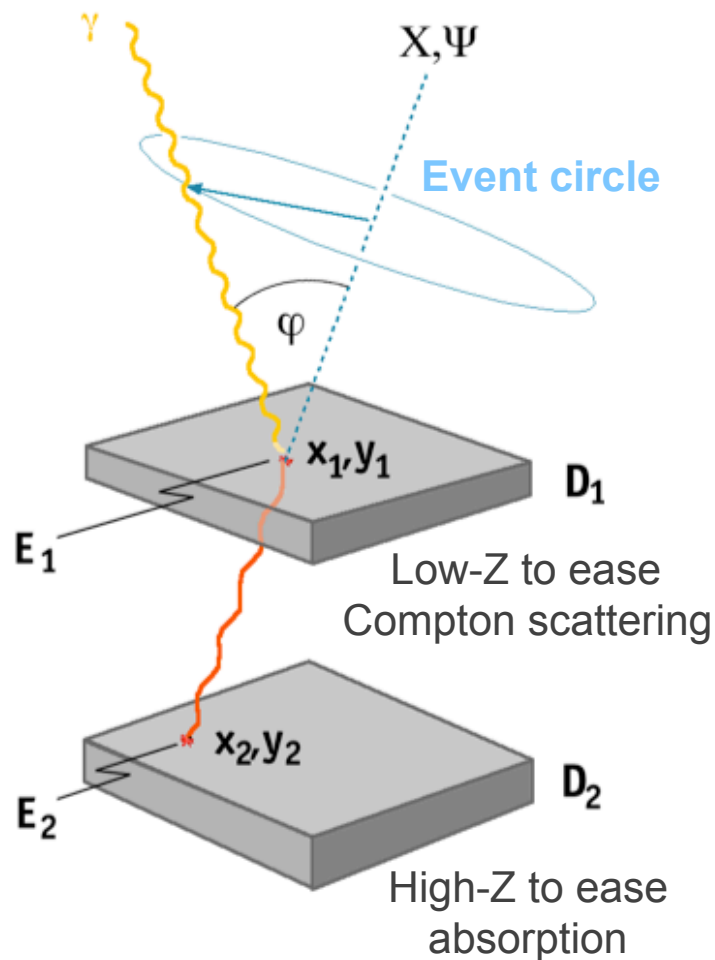
Two-level instruments

1st level: the γ -ray Compton scatters off an electron in a **liquid scintillator**. The scattered photon enters into a **2nd level scintillator** (NaI) and is absorbed. Phototubes can determine the interaction points at the two layers and record the amount of energy deposited in each layer.

It is possible to reconstruct the angle of incidence the photon made wrt the original direction using the **Compton scattering law**, linking this angle and the energy of the scattered photon (2nd level) and the scattering electron (1st level).

“Event circle” (ring on the sky), poor angular resolution (but multiple photons can help to reconstruct the position)

The Compton telescopes: COMPTEL onboard CGRO. II



measured parameters :

- x_1, y_1 : interaction location in D_1
- E_1 : energy deposit in D_1
- x_2, y_2 : interaction location in D_2
- E_2 : energy deposit in D_2
- $t, \Delta t$: arrival time, TOF D_1 - D_2

derived parameters :

- $x_1, y_1, x_2, y_2 \Rightarrow \chi, \psi$
- $E_1, E_2 \Rightarrow \bar{\phi}$

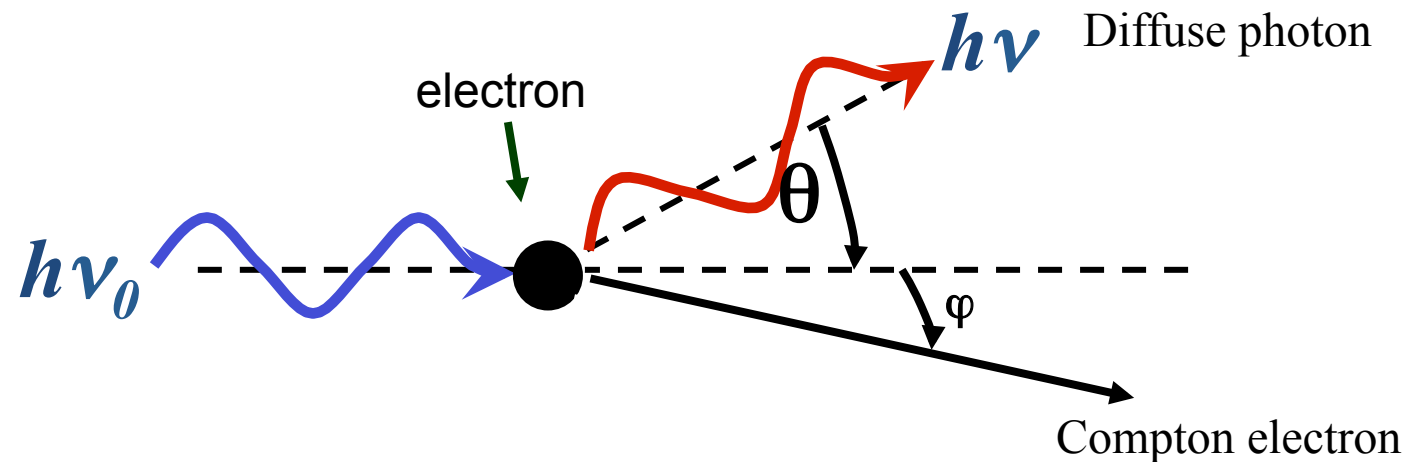
$$\cos \phi = 1 - m_e c^2 \left(\frac{1}{E_2} - \frac{1}{E_1} \right)$$

encoding of the two dimensional source distribution into a 3-D dataspace (X, Ψ, ϕ)

Compton scattering (diffusion)

The photon, after the interaction, has a longer wavelength (i.e., lower frequency, hence energy) wrt. the incident photon

The difference is given to the electron in the form of kinetic energy



Compton wavelength: $h/(m_e c)$

Frequency change

$$\frac{1}{\nu} - \frac{1}{\nu_0} = \frac{h}{m_e c^2} (1 - \cos\theta)$$

Aperture modulation telescopes:

Slat Collimators

Scanning Grid Collimators

Rotation Modulation Collimators

Coded masks Telescope

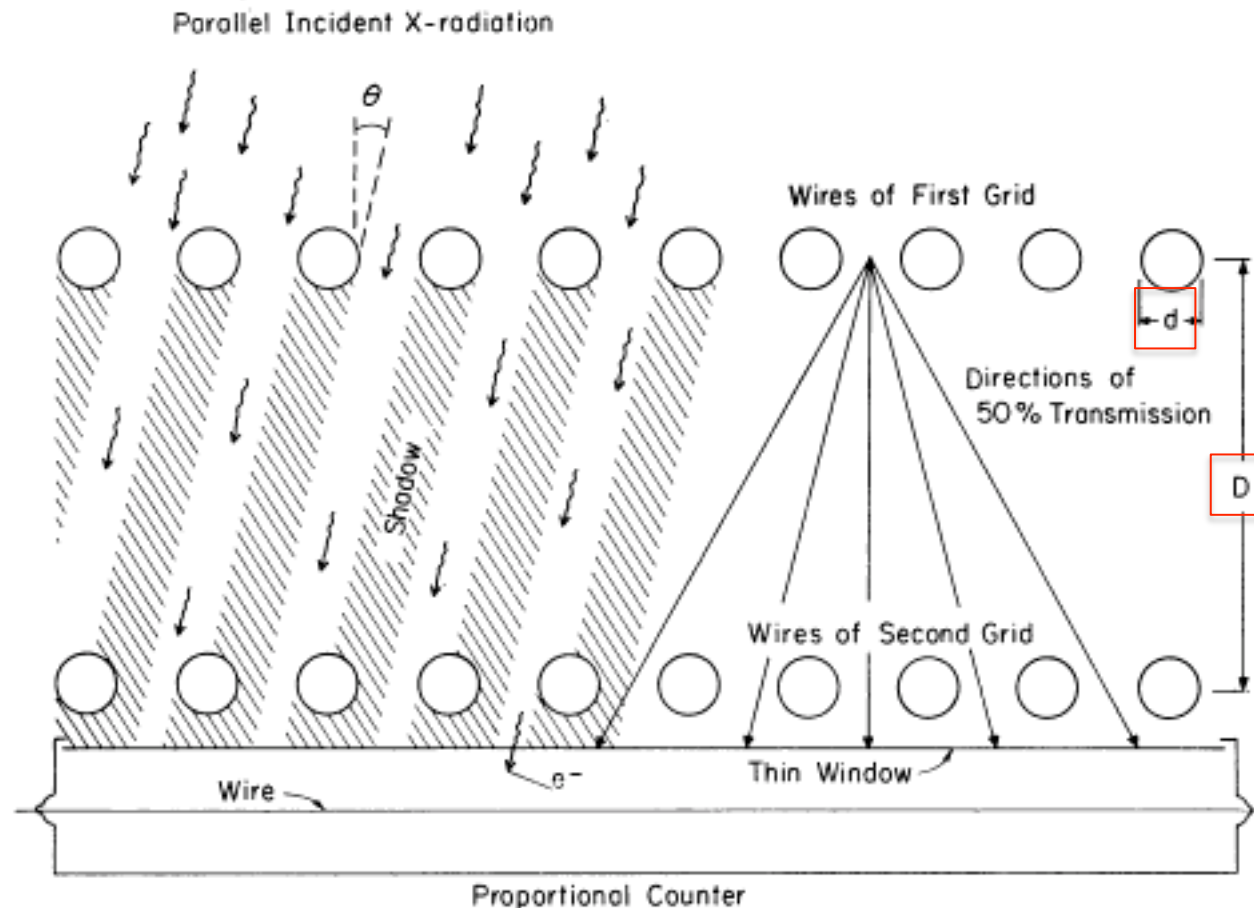
Aperture modulation collimators. I

Slat collimators

- Tested with the first X-ray detectors (proportional counters and inorganic scintillation counters)
 - At first: **slat collimators** (consisting of parallel magnetic plates in front of the detector)
 - The *source* is *modulated* by the *triangular response function* of the *collimator*
- Imaging through aperture modulation, following the original idea by *M. Oda* (**bigrid collimator**)

Aperture modulation collimators. II

Slat collimators

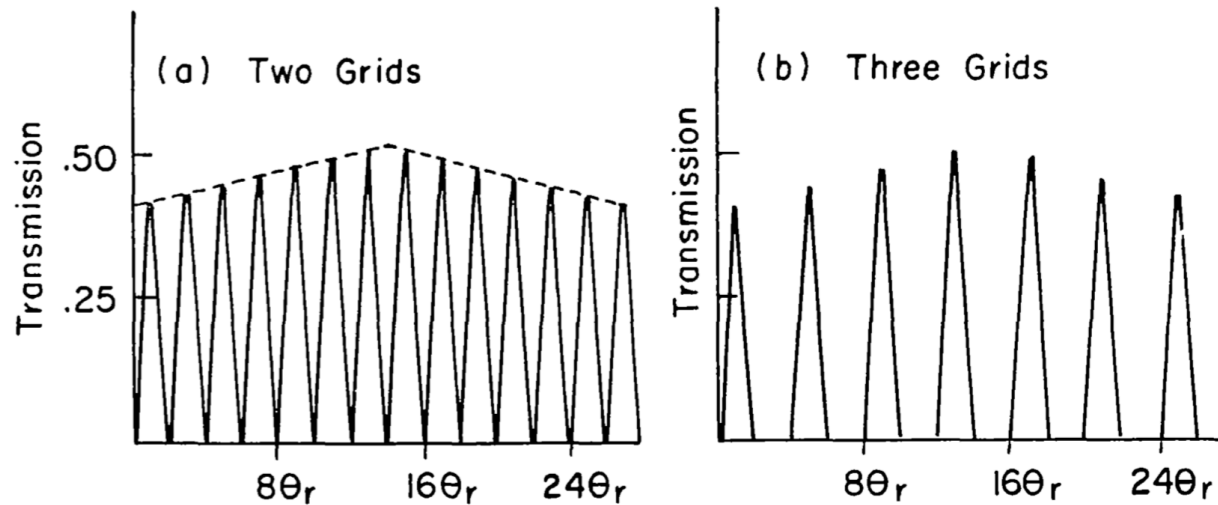


Bigrid modulation collimator
Bradt et al. (1968)

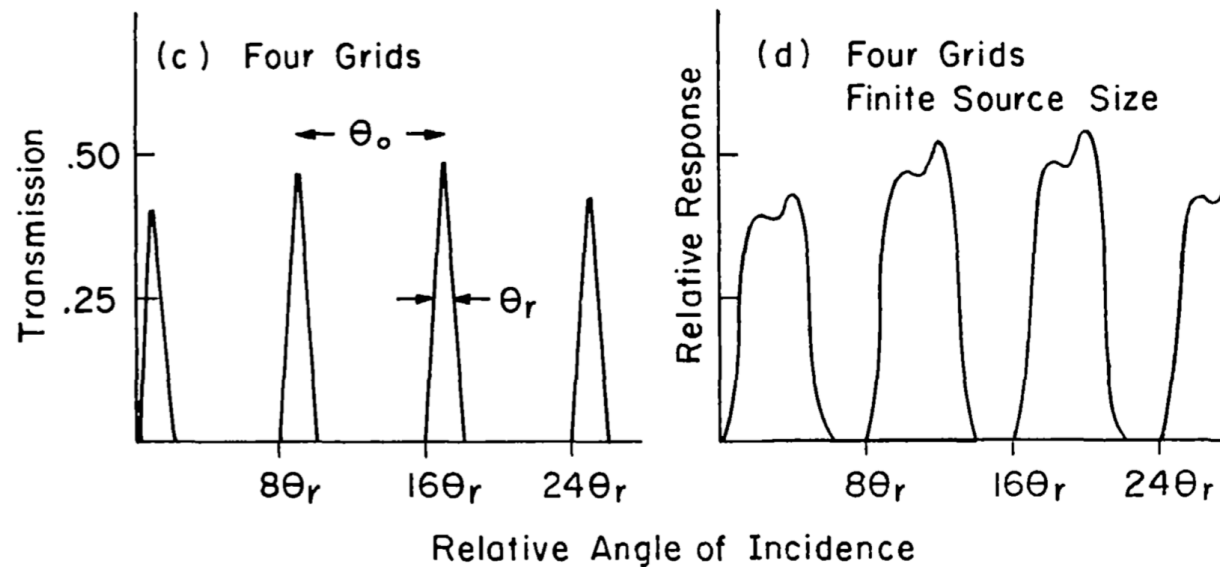
Cells or slits placed in front of the detector. Regions of the detector are blocked to X-ray radiation by the shadows of the grid. The net angular response is triangular and 'cyclic'. No modulation if the source size is $\geq 2d/D$

Aperture modulation collimators. III

Slat collimators

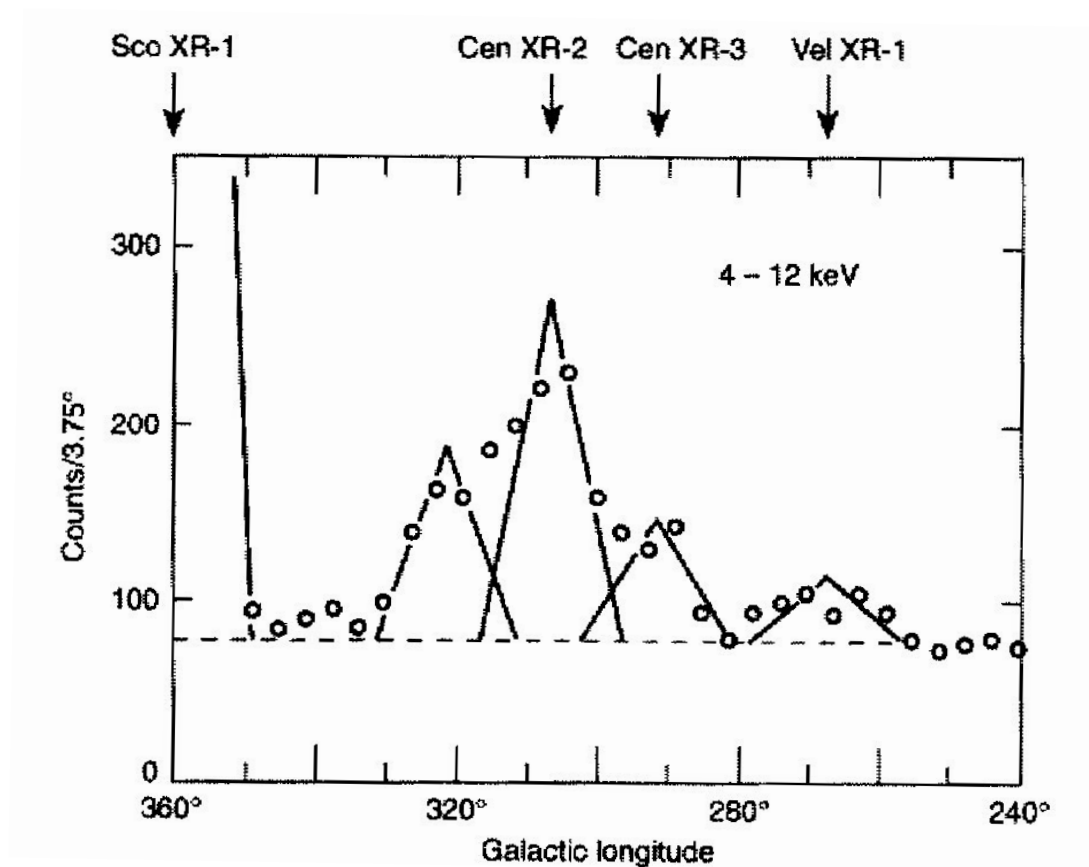


$\Theta_r = d/D$
Possibility to estimate the size of a source



Aperture modulation collimators. IV

Slat collimators

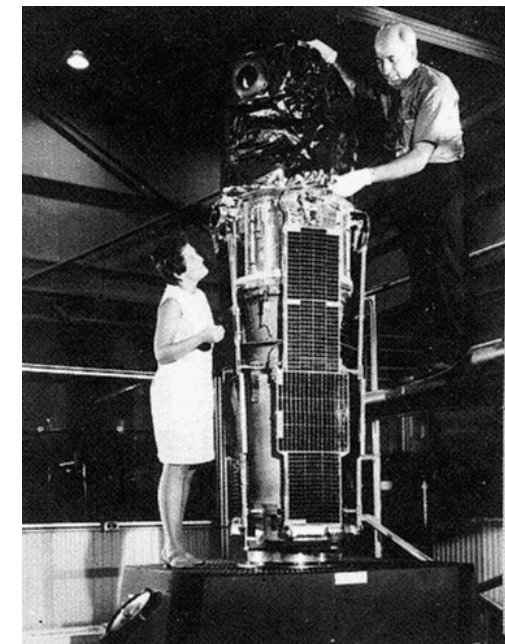
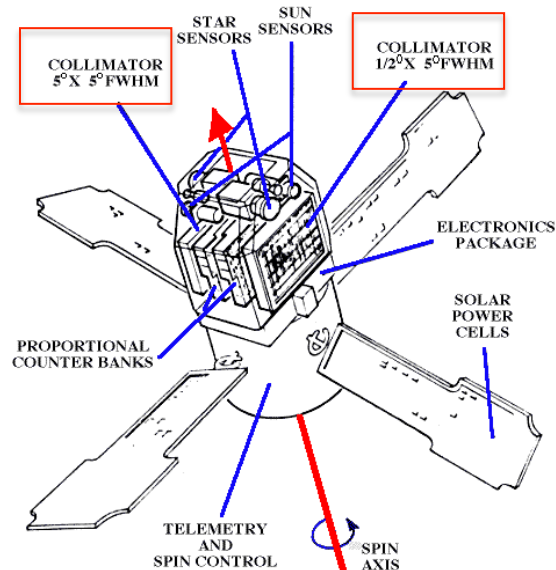


1967 rocket-borne proportional counter
Slat collimator (triangular response)
 $\text{FoV} = 10^\circ \times 30^\circ$

Aperture modulation collimators. V

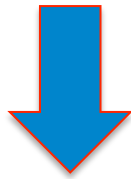
Scanning grid collimators

- Imaging the sky with non-imaging X-ray instruments as a goal
- Linear scanning means position is determined in one direction
- At least a second scanning, preferentially in the direction perpendicular to the previous one
- First all-sky survey in X-rays by *UHURU* (*SAS-1*, 1970-73), 2 proportional counters ($2\text{--}20\text{ keV}$) with metal collimators ($0.5^\circ \times 5^\circ$, $5^\circ \times 5^\circ$ FWHM resolution)



Background subtraction. I

Background subtraction may be a problem for non-imaging instruments

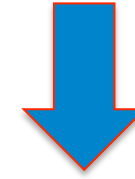


On-off technique

Observation of the source (ON)
minus
observation where the
source is clearly outside the response
of the collimator (OFF)

Result: **SOURCE FLUX = ON – OFF**

Problems: contaminating sources?
Examples: *RXTE*/HEXTE,
BeppoSAX/PDS



Modelling the background

Technique: repeated observations of
background (i.e., ‘source-free’)
regions under different conditions

Examples: *RXTE*/PCA, *Suzaku*/HXD

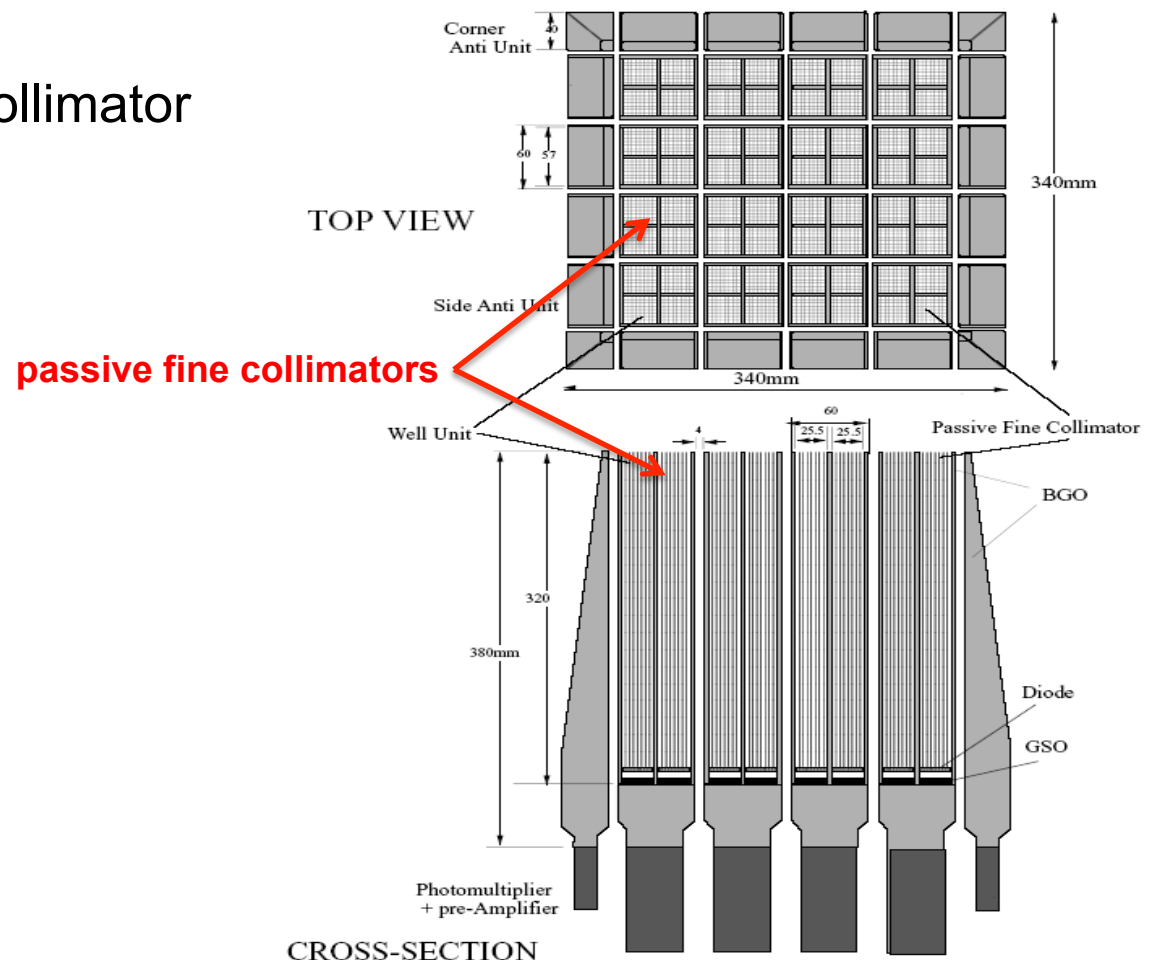
Result: **SOURCE FLUX = ON – OFF
(modeling of the background)**

Background subtraction. II

Suzaku/HXD (hard X-ray detector)

The case of modelling the background with repeated observations of sky ('source-free') regions

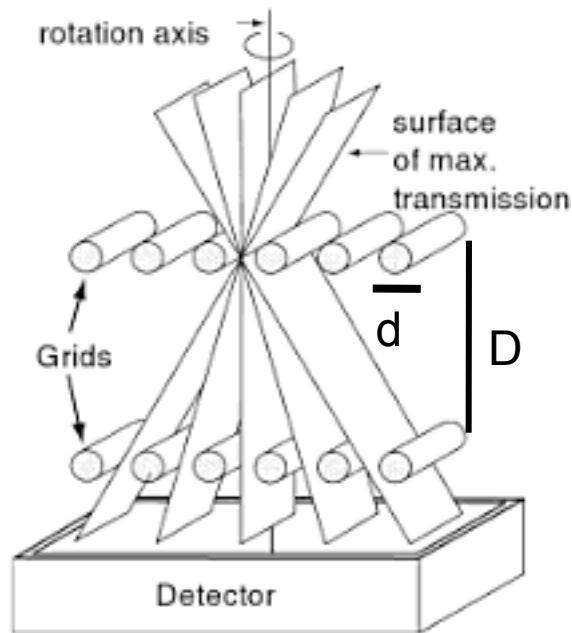
- Active shields and coarse collimator (BGO)
- Detector: GSO (Gd_2SiO_5)
- 8×8 cells (BGO-shielded):
 - $4.6^\circ \times 4.6^\circ$ (FWHM)
- Collimator fine (Bronzo):
 - $0.57^\circ \times 0.57^\circ$ (FWHM)
- 186 kg
- Orbit:
 - 550 km
 - 31°



Aperture modulation collimators. VI

Scanning grid collimators

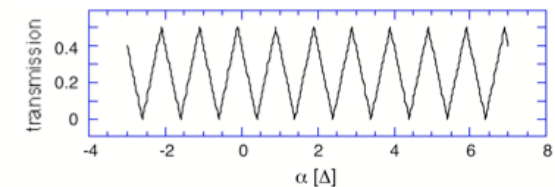
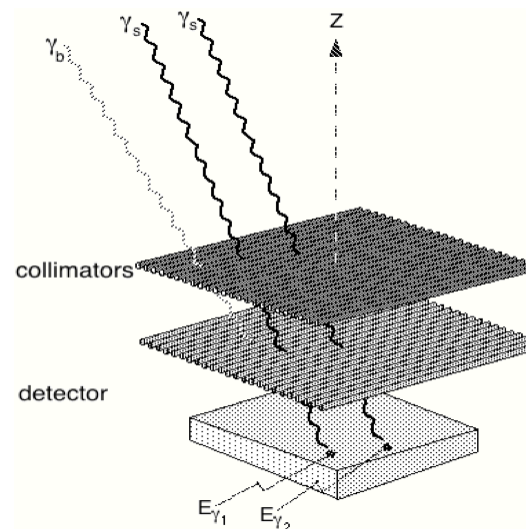
- Two or more planes ('grid of absorbing rods') collimators to improve angular resolution
- Higher resolution with three or more grids (e.g., 4 in the case of HEAO-1 A-3 experiment)
- **Two-dimensional measurements need scans in two or more directions**



Double-grid collimator

Transmission Function of triangular shape

Angular resolution: d/D

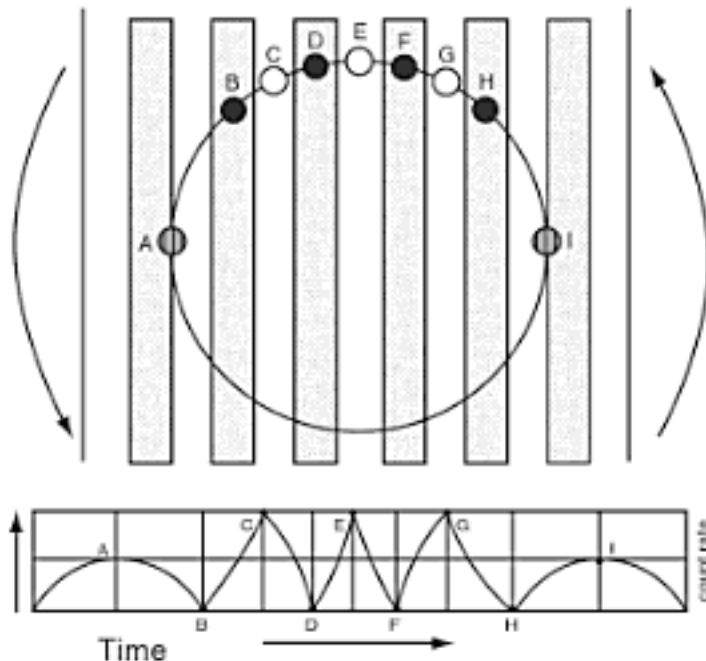


Modulation curve

Aperture modulation collimators. VII

Rotation modulation collimators

- A combined measurement of both coordinates (hence imaging) is possible if a double-grid collimator is *rotated* at a constant velocity around its optical axis
- The resulting source flux is modulated in a unique way
- Multiple sources produce a superposition of response curves which need to be compared with the theoretical one (to understand the possible relative contribution of each source)



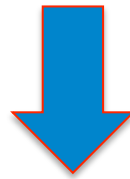
Rotation Modulation Collimator (RMC)

Modulation curve

Spatial aperture modulation.

The way to coded-masks

Alternative to temporal modulation, the spatial aperture modulation requires two position-sensitive detectors. The spatial modulation is achieved by a pattern of 'holes' in an otherwise absorbing plate, providing a **unique spatial code**



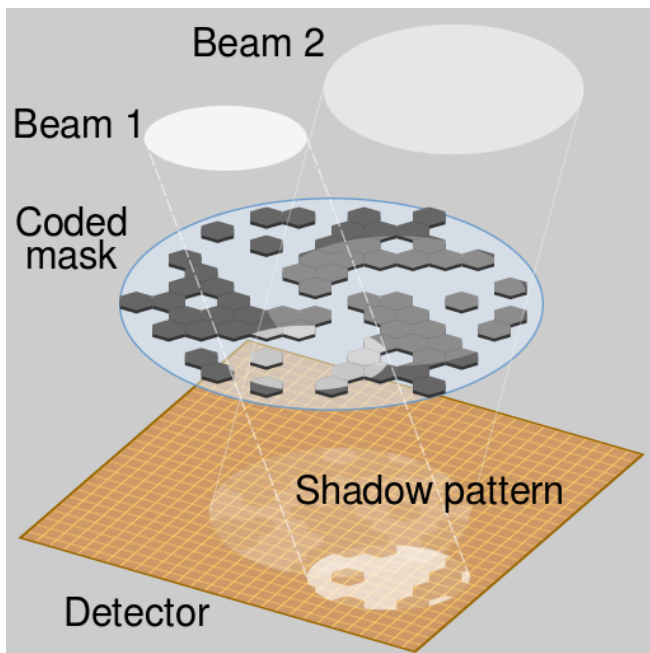
Coded-aperture (coded-mask) telescopes

Working principle: the mask pattern (in the form of the shadow produced by the parallel beam of an X-ray source) is recognized by the two-dimensional position-sensitive detector. Any shift in the pattern is related to a shift of the source position.

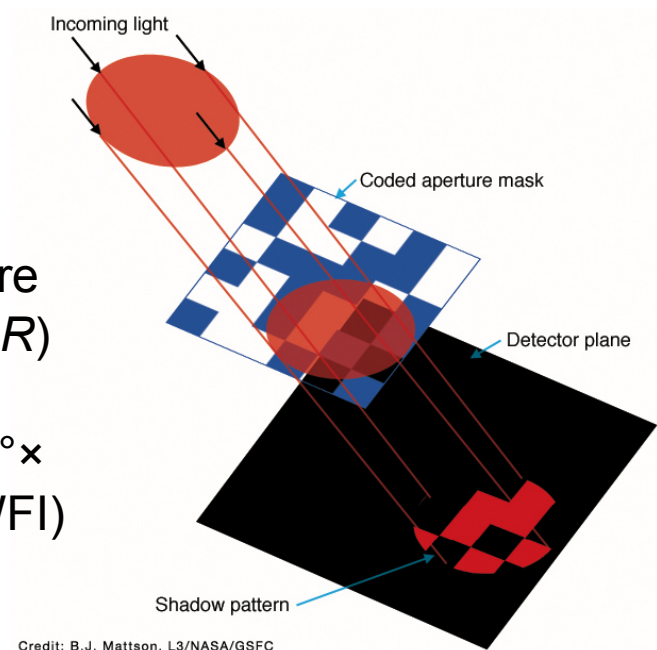
Coded-aperture imaging. I

Coded-masks are plates with areas which are either transparent or opaque to X-ray photons, and are coupled to position-sensitive detectors

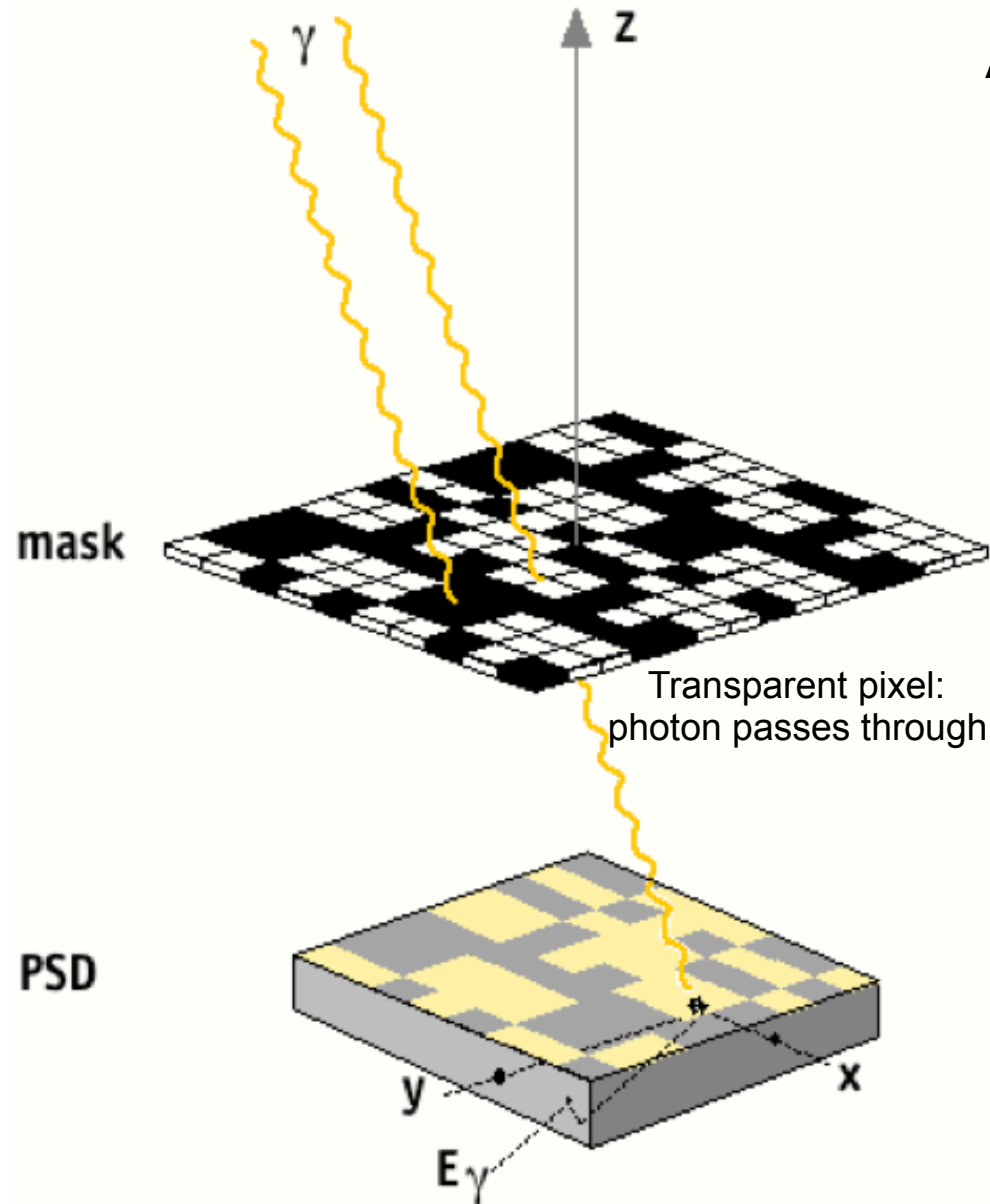
- Photons from a certain direction in the sky **project** the mask (its '**shadow**') on the detector
- Each part of the detector may detect photons incident from any position within the observed sky
- The accumulated *detector image* may be *decoded* to a *sky image* by determining the strength of every possible shifted mask pattern



- Imaging hard (>10 keV) photons (before the advent of *NuSTAR*)
- Large FoV (e.g., $40^\circ \times 40^\circ$ for BeppoSAX/WFI)

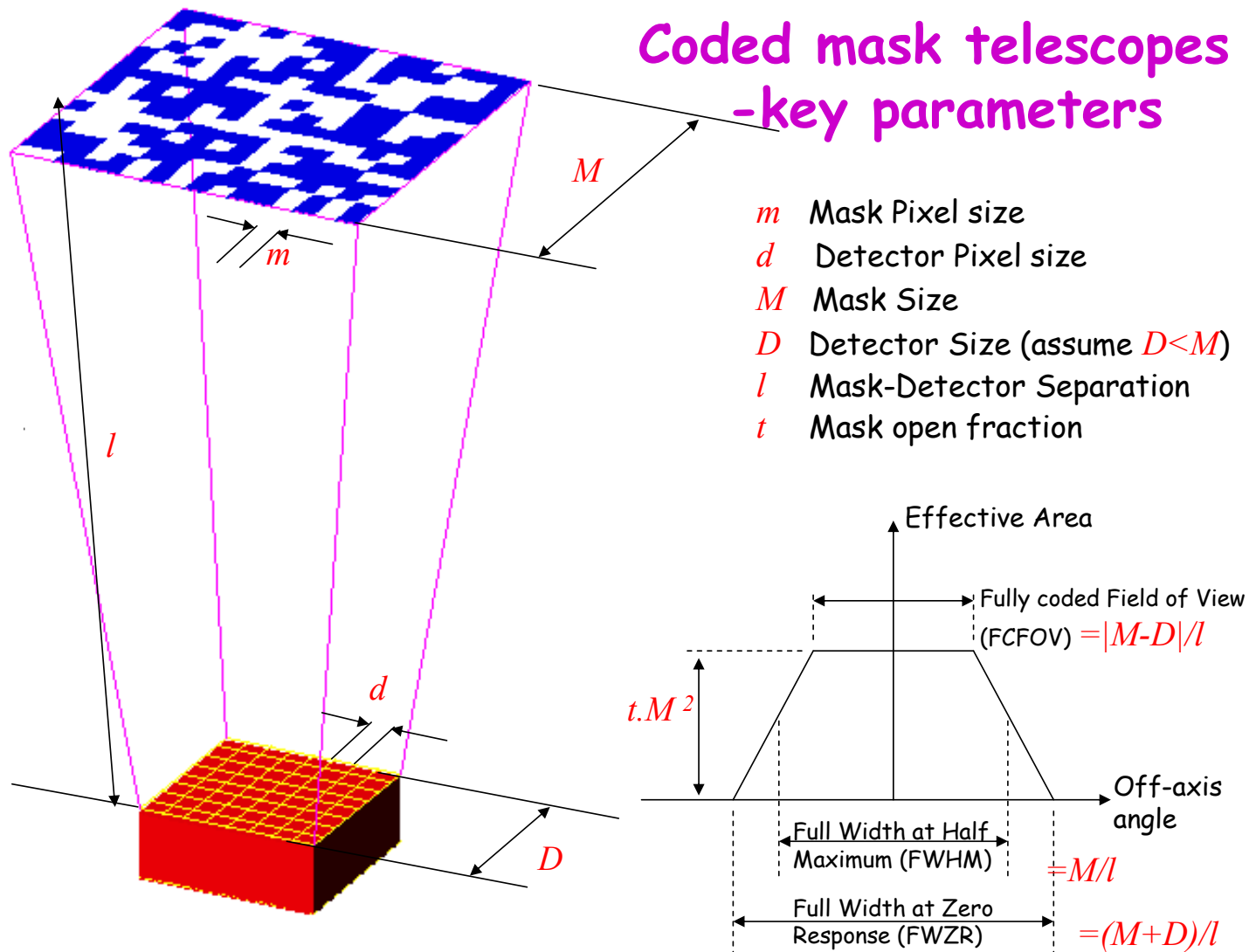


Coded-aperture imaging. II



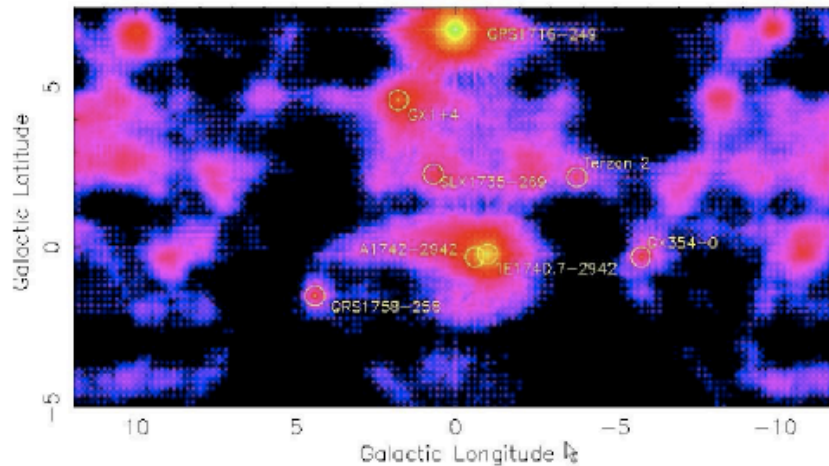
A point source projects a shadow of the mask onto the detection plane.
The distribution of interaction locations is called *shadowgram*

Coded-aperture imaging. III



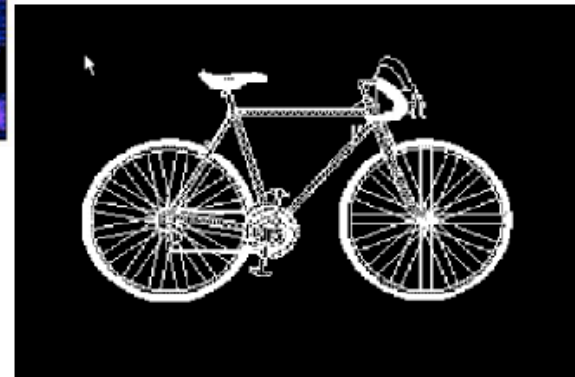
Coded-aperture imaging. IV

Masks are subject to particular 'rules' (see following slides about tuning of the masks)
but any kind of mask can be potentially used



Galactic Center simulation

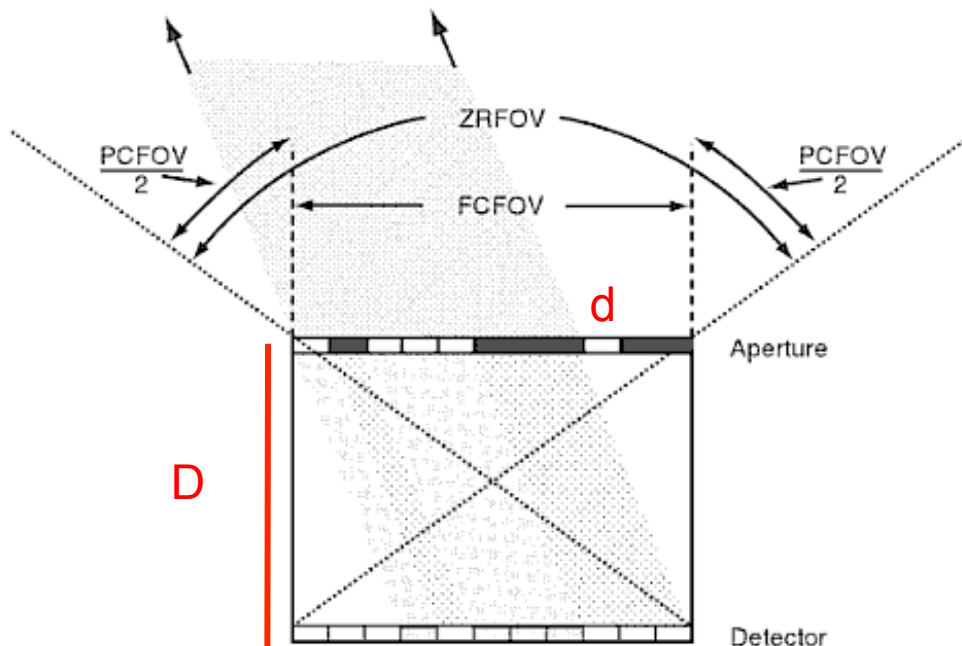
Adopted mask



Coded-aperture imaging. V

Fully-Coded Field of View (FCFOV)

Partially-Coded Field of View (PCFOV)



Full coding is achieved only for on-axis sources in FCFOV

Detector resolution should match the mask element dimension

Fully-coded Field of View (FCFOV)

Photons from any source within this area of the sky cannot reach the detector without passing through the mask (i.e., the entire detector surface is “coded”)

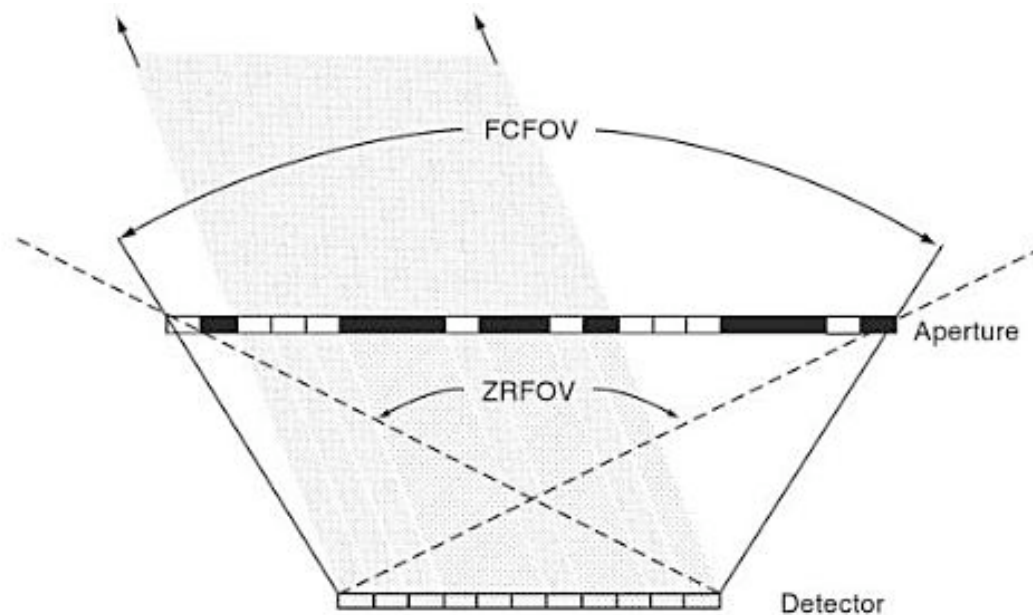
FCFOV for on-axis sources only

$$\text{RESOLUTION} = d/D$$

where d = length of the mask pattern (width of the holes) and D = distance mask-detector

Photons can arrive from sources outside the FCFOV → **partially coded FoV (PCFOV)**: only part of the mask is projected on the detector plane

Coded-aperture imaging. VI



Extension of the FCFOV
through a larger mask
with a repeated pattern

FCFOV achieved also for
off-axis sources

Four parameters defining a coded mask

- (1) Dimension of the mask elements (pixels) – angular resolution
- (2) Number of pixels
- (3) Fraction of open pixels – 50% optimum for backg-dominated observ.
33% otherwise
- (4) Coding pattern – mathematical construction procedures

Coded-aperture imaging. VII

Image reconstruction

The observed intensity distribution over the detector must be interpreted (“unfolded”) using the **coding function** associated with the **mask pattern**

$$D(x) = M(x) \times S(x)$$

D(x)=observed detector distribution

M(x)=coding function (aperture modulation function)

S(x)=sky distribution

$x=(X,Y)$ in the respective plane

D(x) must be inverted to get S(x)

S(x) not unambiguously defined, main problem coming from Poisson statistics because of the presence of background (often dominant over the source signal)

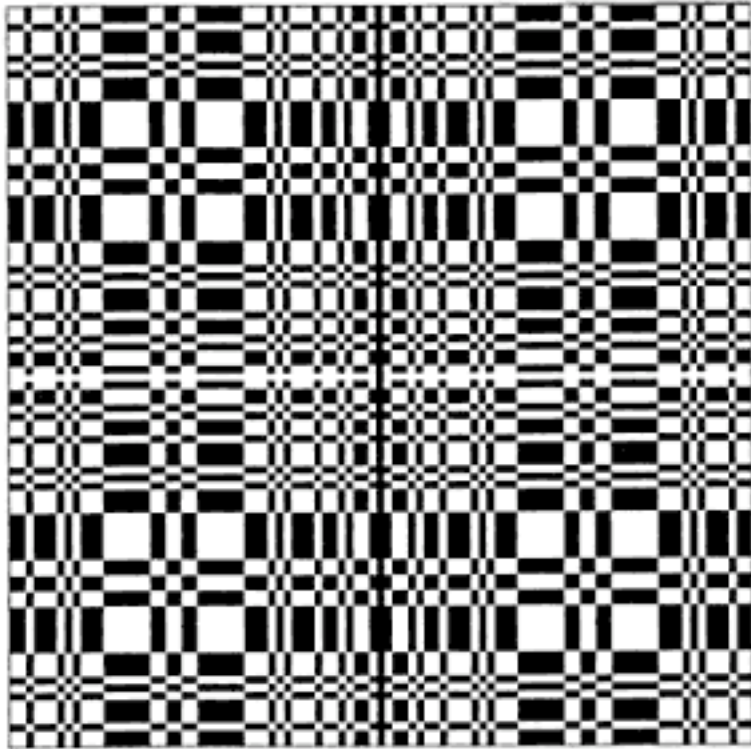
→ $S(x) = B_{\text{sky}}(x) + \sum(S_i(x))$ = X-ray background + all the i sources in the FoV, both coded by M(x)

+ detector background (charged particles, secondary photons)

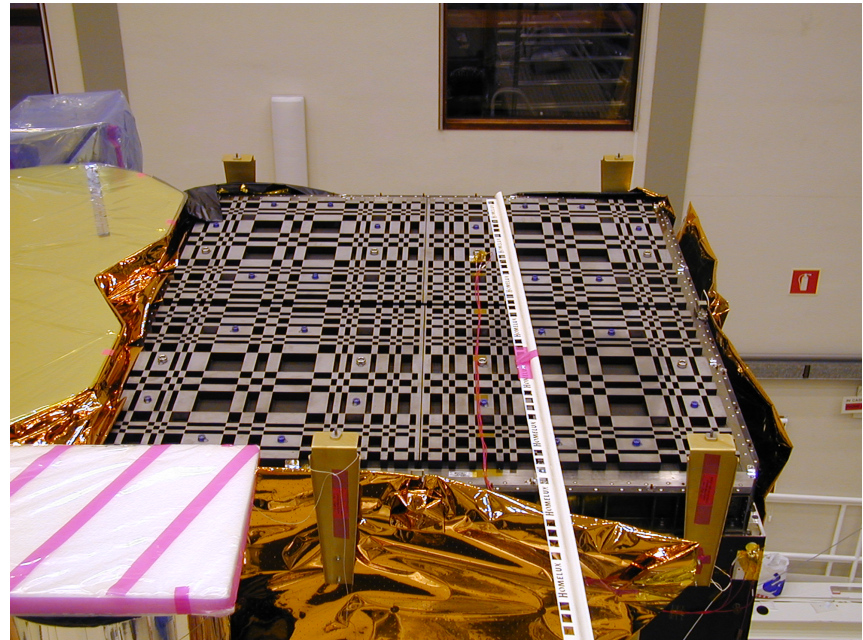
M(x) directly inverted only for few mask patterns

Typically used correlation procedures=correlation of the aperture code with the suitably binned intensity distribution; mismatched filtering=FT⁻¹ of the PSF; backprojection=the mask pattern is projected onto the sky, marking all areas from which the photon could have arrived.

Coded-aperture imaging. VIII

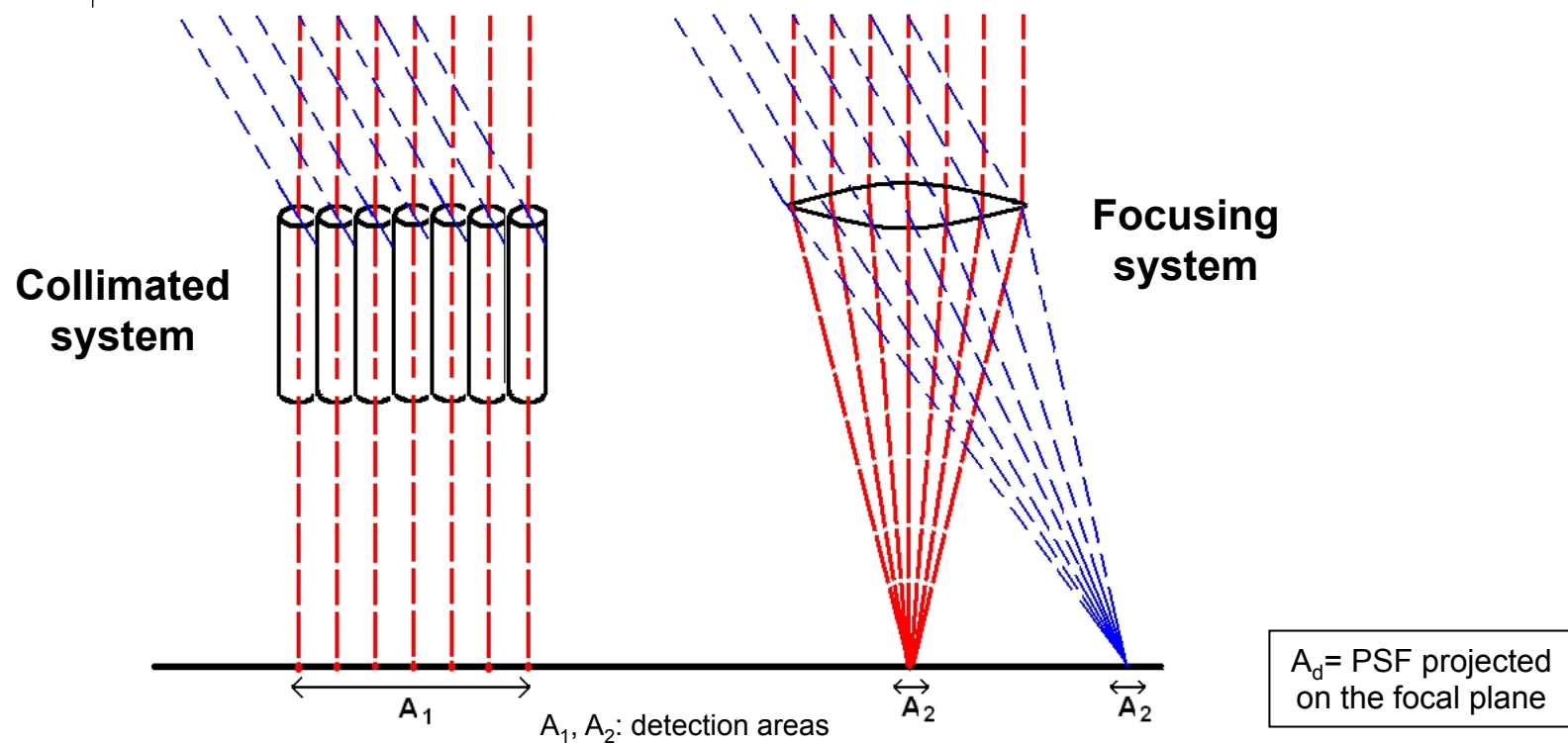


Mask of IBIS (15 keV– 10 MeV)
onboard *Integral*



Collimators vs. Focusing telescopes

Collimator vs. Focusing system. I



$$S_{\min} \approx \frac{n_{\sigma}}{\epsilon_E} \frac{\sqrt{2B}}{\sqrt{A \Delta T \Delta E}}$$

$$S_{\min} \approx \frac{n_{\sigma}}{\epsilon_E} \frac{1}{A_{\text{eff}}} \sqrt{\frac{2B A_d}{\Delta T \Delta E}}$$

In focusing systems, the detection area in the focal plane is largely reduced wrt. a collimator system →
The focusing system can be seen as a concentrator (by a factor A_1/A_2)

In focusing systems, the background signal coming from sky regions unrelated to the source is strongly limited

Collimator vs. Focusing system. II

$$C_B = B A \Delta T \Delta E$$

Background counts from a **collimated telescope** with detector area A, sensitive over the band ΔE , in a time interval Δt , producing a flux B

$$\sigma(C_B) = C_B^{1/2}$$

The counts obey the Poisson statistics

$$C_S = S_E A \Delta T \Delta E \epsilon_E$$

Source counts with flux S_E in the same conditions (QE= ϵ_E)

$$C_{\text{meas}} = (C_S + C_B) - C_B$$

Measured counts (background-subtracted)

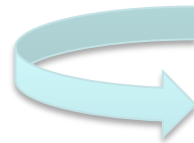
$$\sigma^2(C_{\text{meas}}) = 2\sigma^2(C_B)$$

Background dominates fluctuations

$$S/N = n_\sigma = \frac{C_S}{\sqrt{2C_B}} = \frac{S_E A \Delta T \Delta E \epsilon_E}{\sqrt{2B A \Delta T \Delta E}}$$

Collimator

$$S_{E,\text{min}} = \frac{n_\sigma}{\epsilon_E} \frac{\sqrt{2B}}{\sqrt{A \Delta T \Delta E}}$$



Collimator vs. Focusing system. III

$$C_S = S_E A_{\text{eff}} \Delta T \Delta E \epsilon_E$$

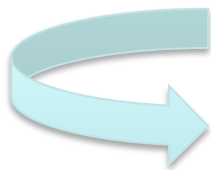
Source counts from a **focusing telescope** with effective area A_{eff} , sensitive over the band ΔE , in a time interval ΔT ; S_E : intrinsic source flux

$$C_B = (B A_d) \Delta T \Delta E$$

Background counts collected onto the PSF spot on the detector (A_d)

$$S/N = n_\sigma = \frac{C_S}{\sqrt{C_S + 2C_B}} \approx \frac{S_E A_{\text{eff}} \Delta T \Delta E \epsilon_E}{\sqrt{2B A_d \Delta T \Delta E}}$$

Case of weak sources ($S < B$)



Focusing

$$S_{E,\text{min}} = \frac{n_\sigma}{\epsilon_E} \frac{1}{A_{\text{eff}}} \sqrt{\frac{2B A_d}{\Delta T \Delta E}}$$

X-ray astronomical optics: history in pills. I

- **1895: Roentgen discovers “X-rays”**
- 1948: First successful focalization of an X-ray beam by a total-reflection optics (Baez)
- 1952: H. Wolter proposes the use of two-reflection optics based on conics for X-ray microscopy
- 1960: R. Giacconi and B. Rossi propose the use of grazing incidence optics for X-ray telescopes
- **1962: discovery by Giacconi et al. of Sco-X1, the first extra-solar X-ray source**
- 1963: Giacconi and Rossi fly the first (small) Wolter I optics to take images of Sun in X-rays
- 1965: second flight of a Wolter I focusing optics (Giacconi + Lindsley)
- **1970: *Uhuru*, the first satellite for X-ray astronomy (no X-ray optics)**
- 1973: SKYLAB carry onboard two small X-ray optics for the study of the Sun
- **1978: *Einstein*, the first satellite with optics entirely dedicated to X-rays**

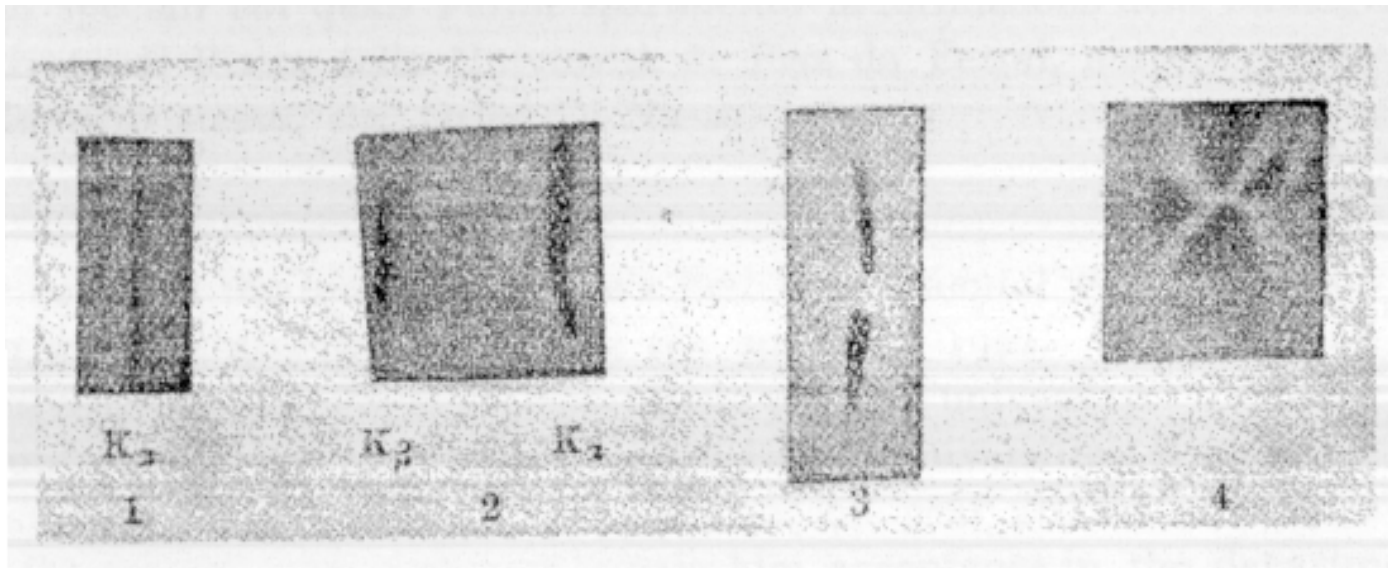
X-ray astronomical optics: history in pills. II

- 1983: *EXOSAT* operated (first European mission with X-ray optics aboard)
- 1990: *ROSAT*, first All Sky Survey in X-rays by means of a focusing telescope with high imaging capabilities
- 1993: *ASCA*, a multi-module focusing telescope with enhanced effective area for spectroscopic purposes
- 1996: *BeppoSAX*, a broad-band satellite with Ni electroformed optics
- 1999: launch of ***Chandra***, the X-ray telescope with best angular resolution, and ***XMM-Newton***, the X-ray telescope with most effective area
- 2004: launch of the *Swift* satellite devoted to the GRBs investigation (with aboard XRT)
- 2005: launch of *Suzaku* with hard X-ray detector
- 2012: launch of *NuSTAR* (with the first X-ray focusing imaging instrument up to 80 keV)
- 2016: launch of *Astro-H/Hitomi* (Japanese mission including a calorimeter) – failed soon

What's Next?

X-ray astronomical optics: history in pills. III

Imaging experiments using Bragg refraction from ‘replicated’ mica pseudo-cylindrical optics



E. Fermi – Thesis Laurea, “Formazione di immagini con i raggi Roentgen” (“Imaging formation with Roentgen rays”), Univ. of Pisa (1922)

Courtesy of Giorgio Palumbo

Reflection of X-rays

X-ray optics. I

X-ray optics are used to

- To achieve the best 2-dim angular resolution
 - To distinguish nearby sources or different regions of the same source
 - To perform morphological studies
- As a collector to “gather” weak fluxes (case of limited photon statistics)
- As a concentrator, so that the image photons may interact in a small region of the detector, thus limiting the influence of the background
- To serve with high spectral resolution dispersive spectrometers such as transmission gratings and reflection gratings
- To simultaneously measure both the source(s) of interest and the contaminating background in other (source-free) regions of the detector

X-ray optics. II

X-ray optical constants

- X-rays are hard to refract or reflect: the refractive index of all materials in X-rays is very close to 1 and only slightly less than 1 → X-rays are above the characteristic energy of bonded e- in atoms
- Complex index of refraction of the reflector to describe the interaction X-rays /matter (see, for a review, Aschembach et al. 1985, Rep. Prog. Phys. 48, 579)
- The amplitude of reflection is described by the Fresnel's equations

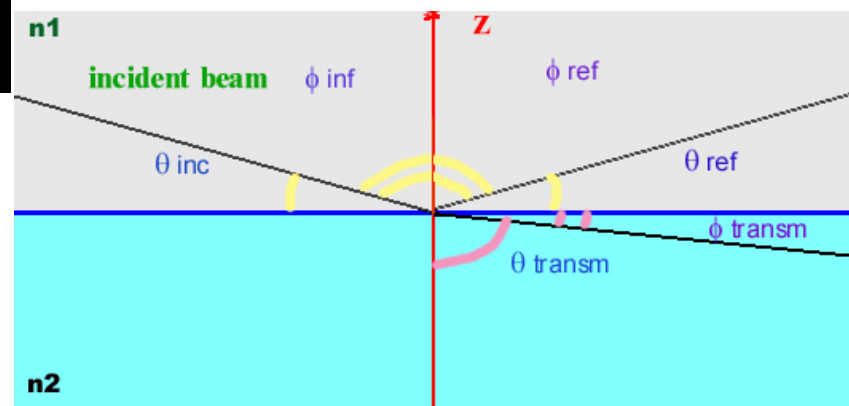
$$n=1-\delta+i\beta$$

where δ describes the phase change and β accounts for the absorption

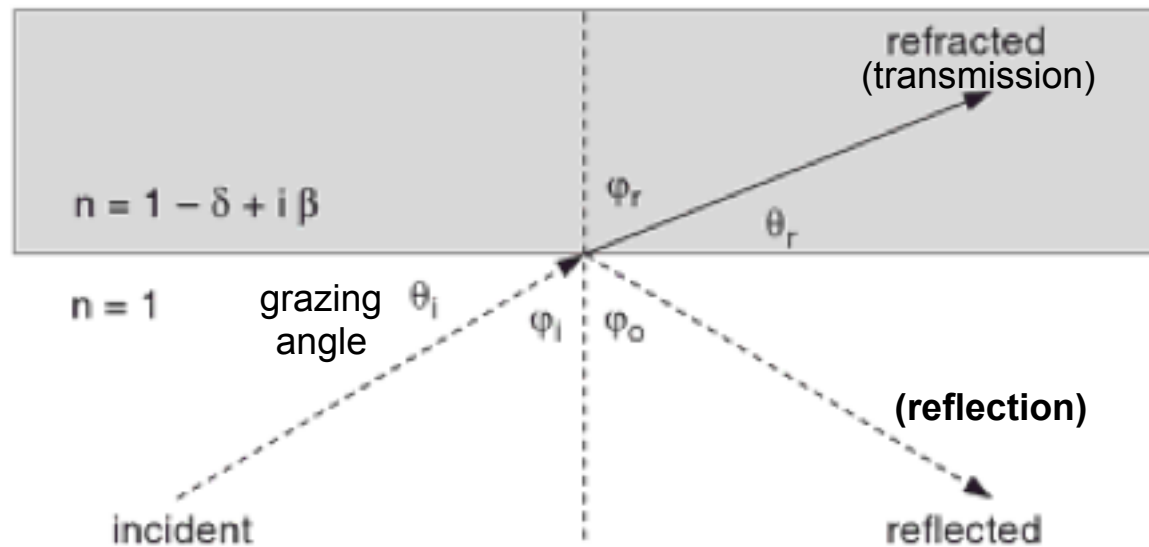
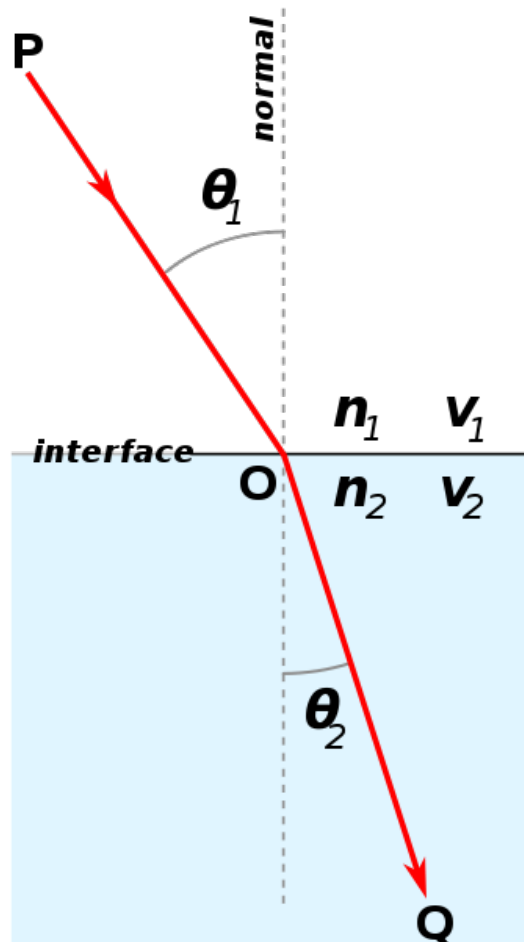
δ and β depend on the wavelength

n: refraction index of the material used for the coating of the optics

Total reflection using grazing incidence + Snell's law



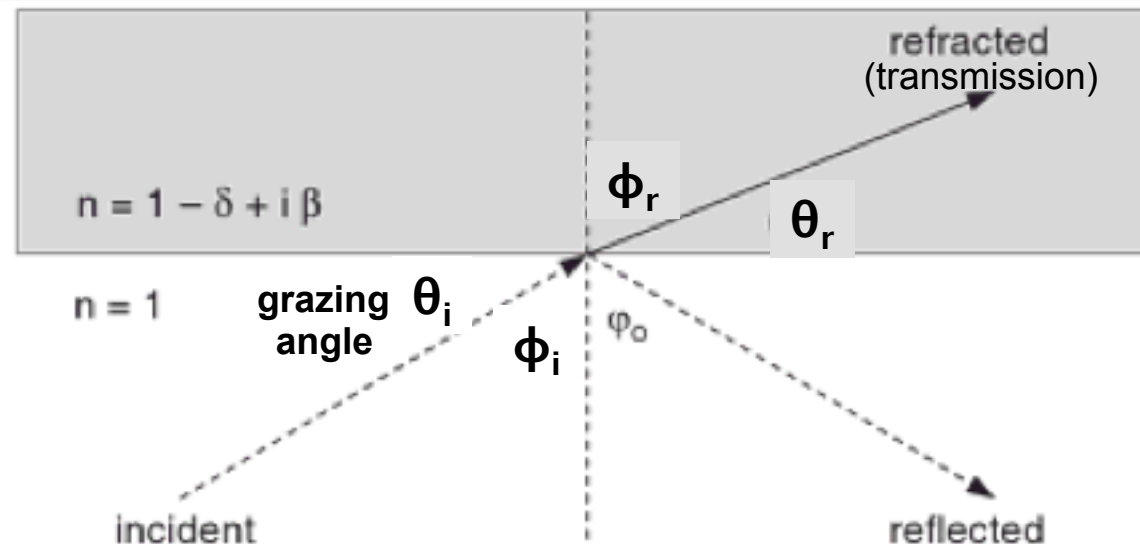
X-ray optics. III



Snell's Law of Refraction:
relationship between the angles of incidence
and refraction in a medium

$$n_1 \sin \theta_1 = n_2 \sin \theta_2$$

X-ray optics. IV



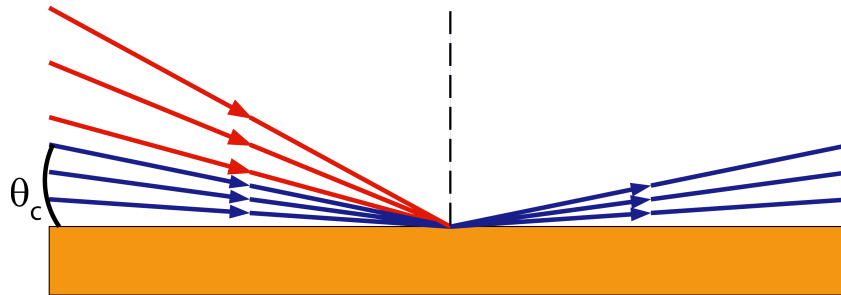
$$\begin{aligned}
 n_1 &= 1, n_2 = (1 - \delta) \longrightarrow \sin \phi_i = (1 - \delta) \sin \phi_r \\
 \theta &= (90 - \phi) \rightarrow \cos \theta = \cos(90 - \phi) = \sin \phi \\
 \phi &= (90 - \theta) \rightarrow \sin \phi = \sin(90 - \theta) = \cos \theta \\
 \cos(90 - \phi_i) &= \cos \theta_i = \sin \phi_i = (1 - \delta) \sin \phi_r = (1 - \delta) \cos \theta_r \\
 \Rightarrow \cos \theta_i &= (1 - \delta) \cos \theta_r
 \end{aligned}$$

Total reflection if no real solution for θ_r
 $\delta > 0, \cos \theta_r \leq 1 \rightarrow$ There is a **critical angle** θ_c below which refraction is impossible
 and total external reflection occurs (**grazing angle**, $\theta_i = \theta_c$)

Extreme case for low θ_r values $\theta_r : \cos \theta_r = 1 - \theta_r^2/2 \approx 1 \rightarrow \cos \theta_i = \cos \theta_C = 1 - \delta$

X-ray optics. V

$$\cos \theta_C = 1 - \delta$$



Total reflection at angles lower than θ_c , the **critical angle**, mostly depending on the **density of the material** used for the optics coating and the **energy of the incoming photon**

The challenge is to be able to use not-too-low critical angles for the grazing incidence of the photon

X-ray optics. VI

$$\cos \theta_C = 1 - \delta$$

- Real part of n slightly less than unity for matter at X-rays (vs. $n=1$ in vacuum); $\delta \ll 1$
- Snell's law ($n_1 \cos q_1 = n_2 \cos q_2$) to find a critical angle for total reflection
- (Total) external reflection in vacuum for angles $<$ critical angle:
- X-ray partially reflected also for $\theta > \theta_{\text{crit}}$; also, some absorption in the material

$$\text{Low angles : } \cos \theta_C = 1 - \frac{1}{2} \theta_C^2 = 1 - \delta \Rightarrow \theta_C = \sqrt{2\delta}$$

Far from fluorescent edges: $\delta \approx \frac{N_0 Z r_e \rho \lambda^2}{2\pi A} \rightarrow \theta_C \approx 28 (\rho Z / A)^{1/2} / E$ (milli-radians)

where N_0 =Avogadro's number
 Z =atomic number
 r_e =electron radius
 ρ =density
 λ =wavelength of the incoming photon
 A =atomic weight

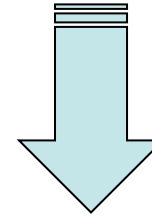
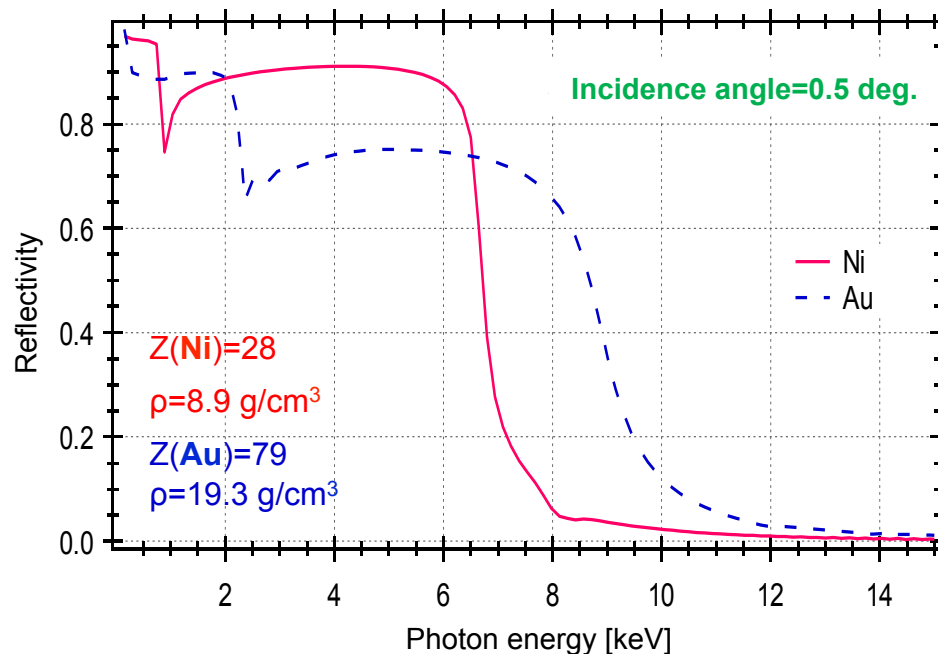
Critical angle

- Inversely dependent on energy
- Higher Z materials reflect higher energies, for a fixed grazing angle
- Higher Z materials have a larger critical angle at any energy

X-ray optics. VII

- For heavy elements, $Z/A \approx 0.5$, and if $\delta \ll 1$:
where $\lambda[\text{\AA}]$ and $\rho[\text{g/cm}^3]$, and $\theta[\text{arcmin}]$

$$\theta_{crit} \approx \sqrt{2\delta} \approx 5.6\lambda\sqrt{\rho}$$



$$\theta_{crit} \propto \sqrt{\rho / E}$$

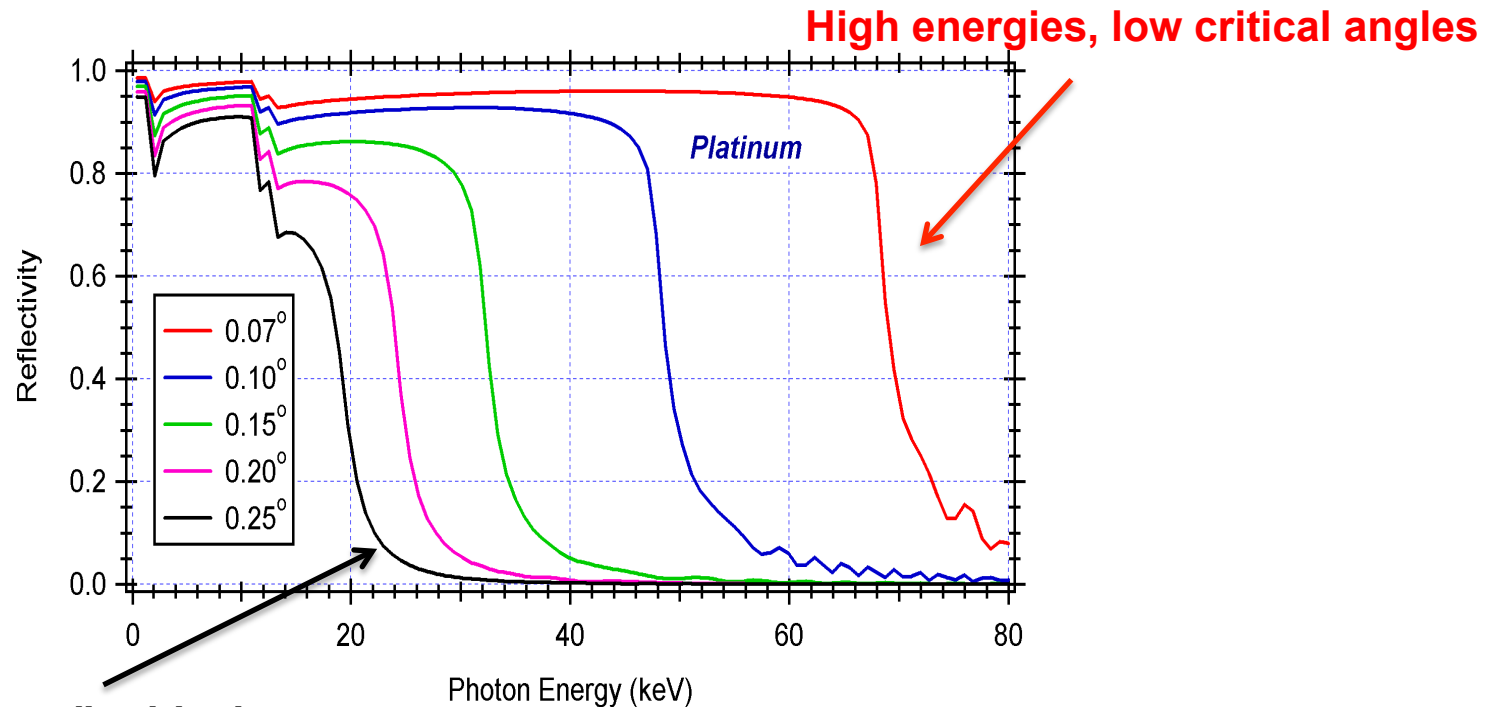
Higher Z materials reflect higher energies, for a fixed grazing angle

- Some reflectivity is lost due to scattering related to the presence of micro-roughness at the surface
- Use of heavy materials (but attention at the absorption edges...)

Condition to be satisfied for total reflection: $\vartheta < \vartheta_c$

X-ray optics. VIII

$$\theta_{crit} \propto \sqrt{\rho} / E$$



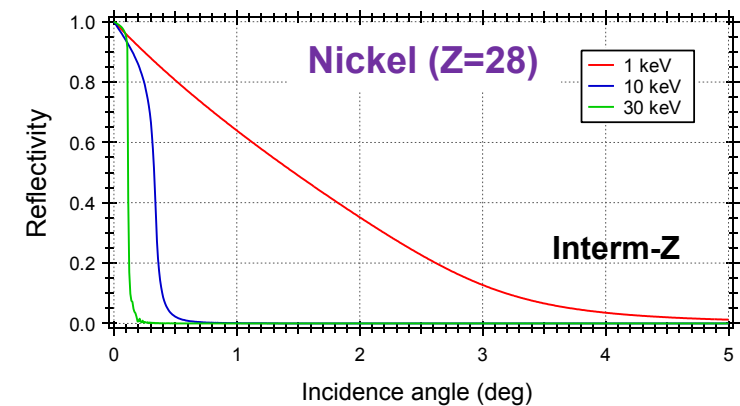
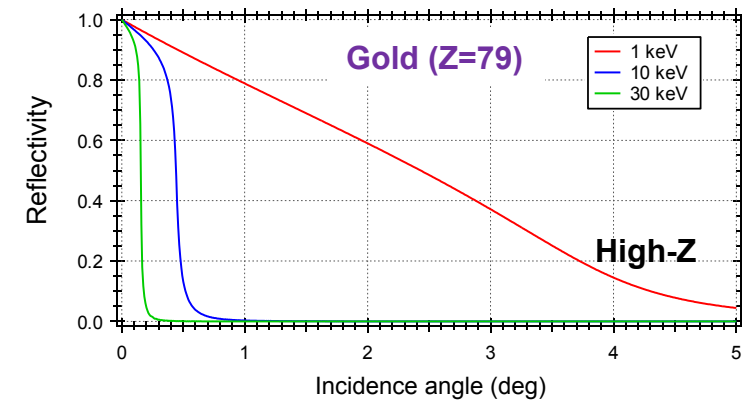
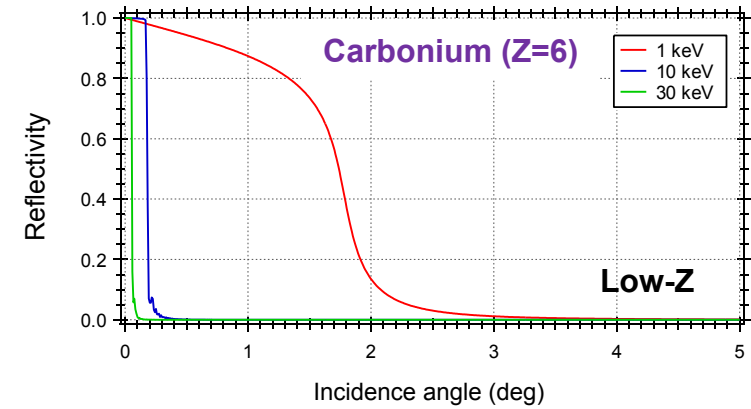
Low energies, “large” critical angles possible

The critical angle for total reflection is higher in case of lower energy photons.
To focus hard X-rays, low θ_{crit} are needed, which is challenging

X-ray optics. IX

$$\theta_{crit} \propto \sqrt{\rho} / E$$

High-Z materials have a large critical angle at any energy



X-ray optics. X

X-ray optical constants for common materials

element	Z	δ	β	θ_c (10 keV)
C (diamond)	6	$4.6 \cdot 10^{-6}$	$4.5 \cdot 10^{-9}$	0.173°
Si	14	$4.9 \cdot 10^{-6}$	$7.4 \cdot 10^{-8}$	0.180°
Cu	29	$1.6 \cdot 10^{-5}$	$1.9 \cdot 10^{-6}$	0.326°
Au	79	$3.0 \cdot 10^{-5}$	$2.2 \cdot 10^{-6}$	0.443°

Grazing reflection and mirror shapes. I

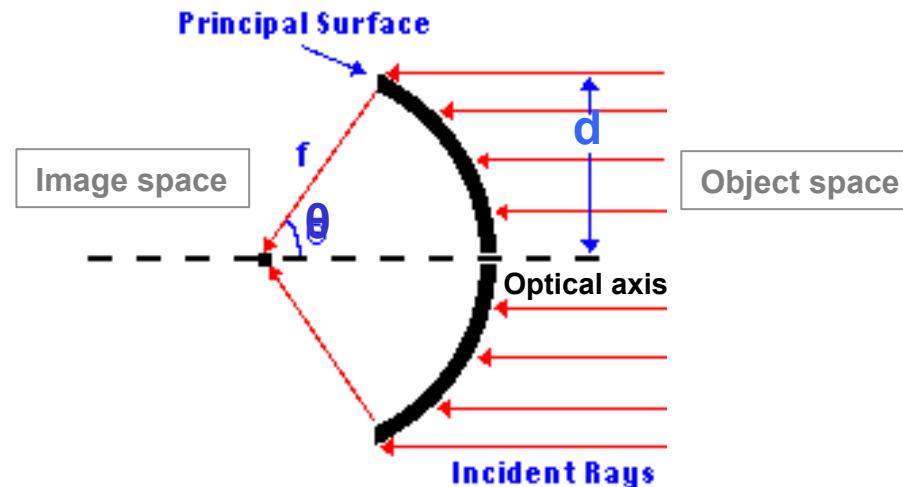
Abbe sine condition: condition that a lens or an optical system must satisfy to produce sharp images (for on-axis and off-axis positions) free from the blurring and distortion caused by coma. It states that an optical system will form an image of an infinitely distant object only if for each ray in the parallel beam emanating from the source:

$$d / \sin \theta = f$$

d: radial distance of the ray from the optical axis

θ : angle of the final path of the ray relative to its initial path (and thus the optical axis)

f: constant for all rays (radius of the 'sphere')



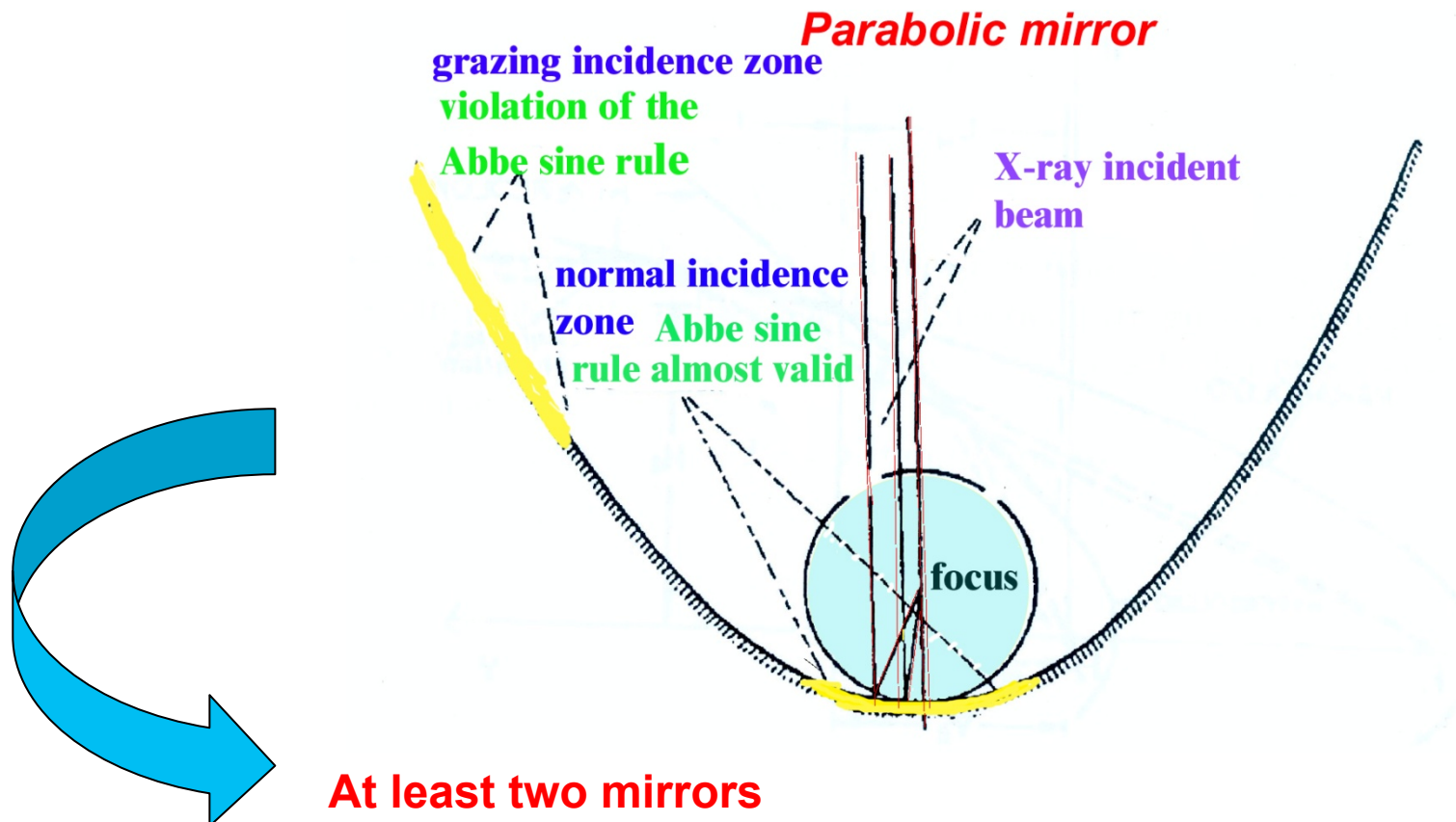
Typical blurring of a focal spot due to coma (off-axis aberration caused by a different magnification of reflected rays, depending on the hitting position at the mirror surface)

An image will be formed if the *principal surface* (*Abbe surface*), defined as the locus of the intersections of the initial and the final paths of rays (i.e., of each incoming ray with its corresponding focused ray), is spherical around the image, with center in the focus.

In other words, the optics' principal surface has to be a sphere making **the distance to the focus f the same for all paraxial rays**. An optical axis satisfying the Abbe sine condition acts as a simple spherical lens.

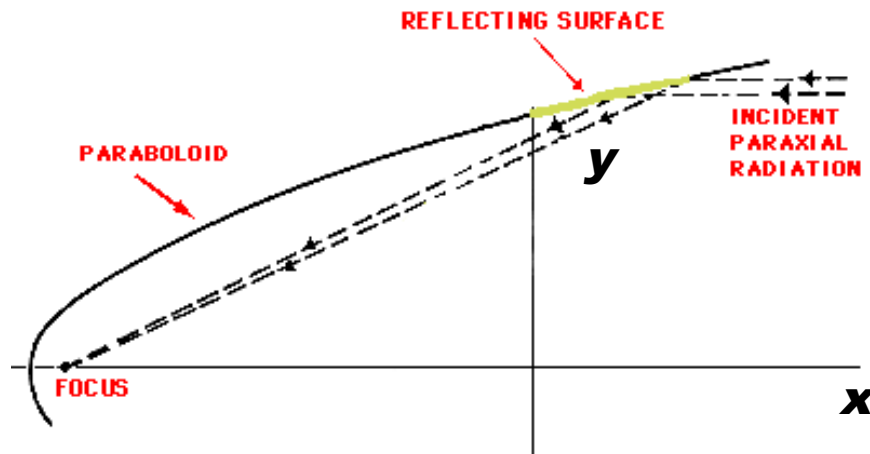
Grazing reflection and mirror shapes. II

Single parabolic mirror: the principal surface is identical to the mirror surface → the sine condition is satisfied if the reflection is almost perpendicular to the mirror surface.
The parabolic profile approximately obeys to the Abbe rule only near the vertex, i.e., at normal incidence, but not for grazing incidence angles
→ the parabolic geometry is not optimal for X-ray telescope design



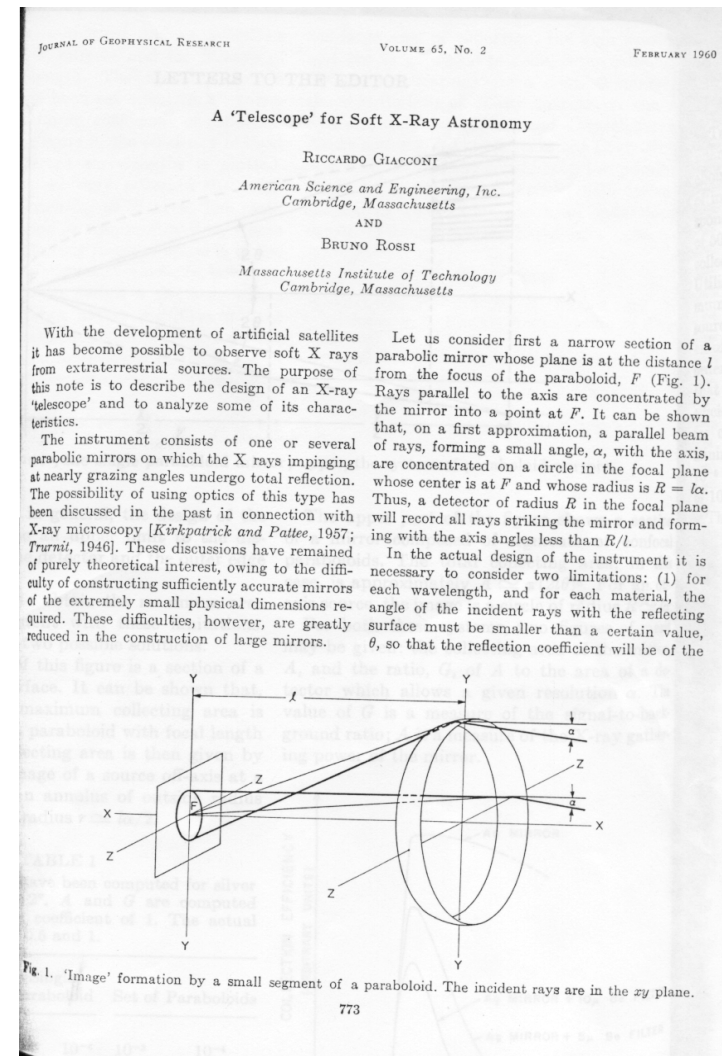
Grazing reflection and mirror shapes. III

X-ray mirrors with parabolic profile



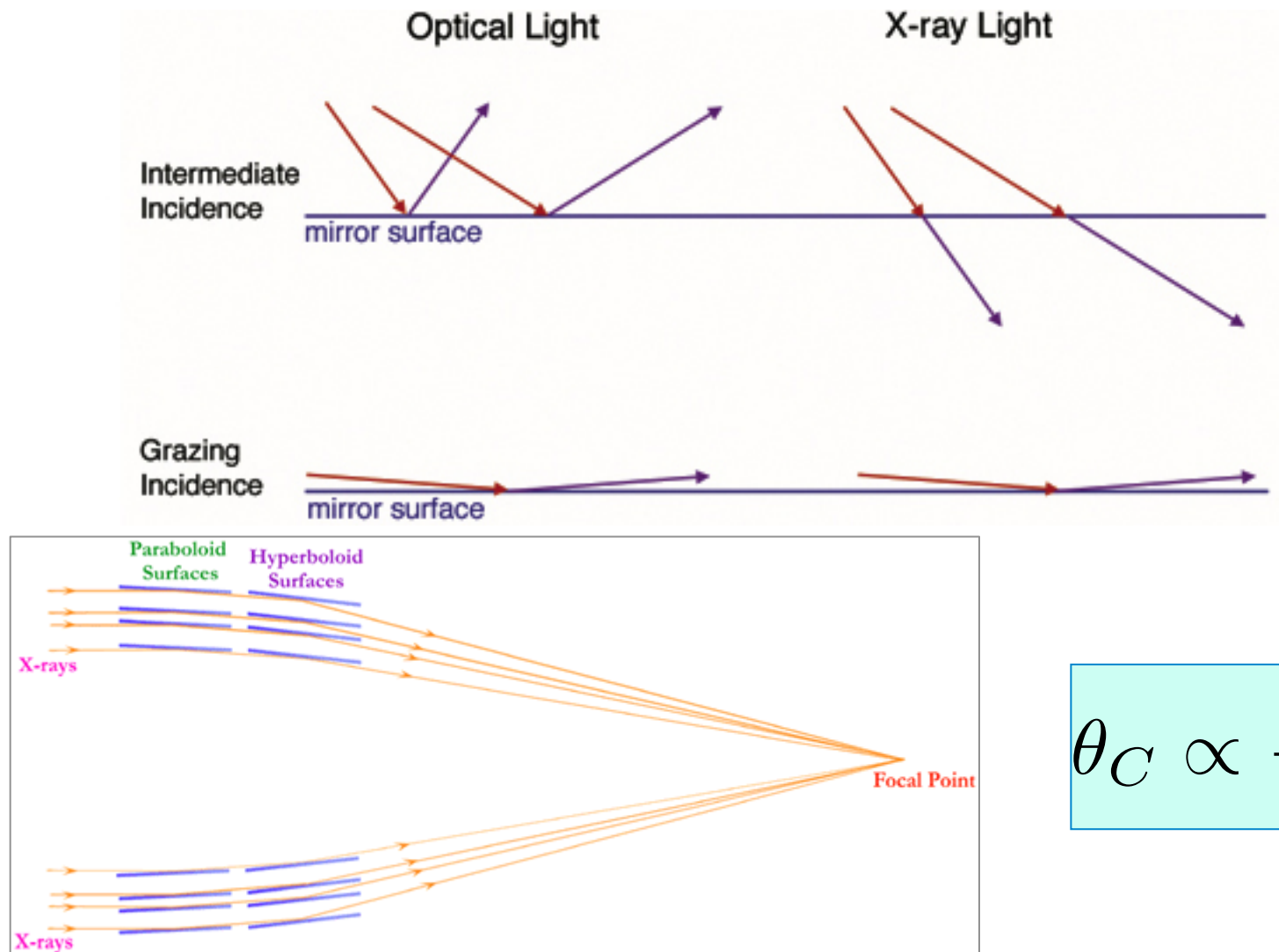
- Perfect on-axis focusing
- Off-axis images strongly affected by coma

Giacconi & Rossi 1960



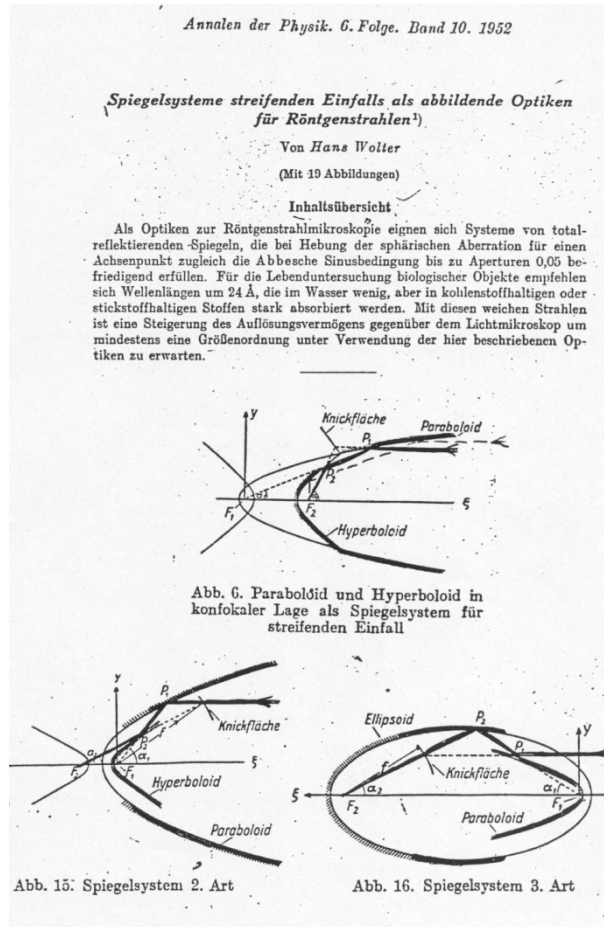
Grazing reflection and mirror shapes. IV

Two mirrors is the solution



$$\theta_C \propto \frac{\sqrt{\rho}}{E}$$

Grazing reflection and mirror shapes. V

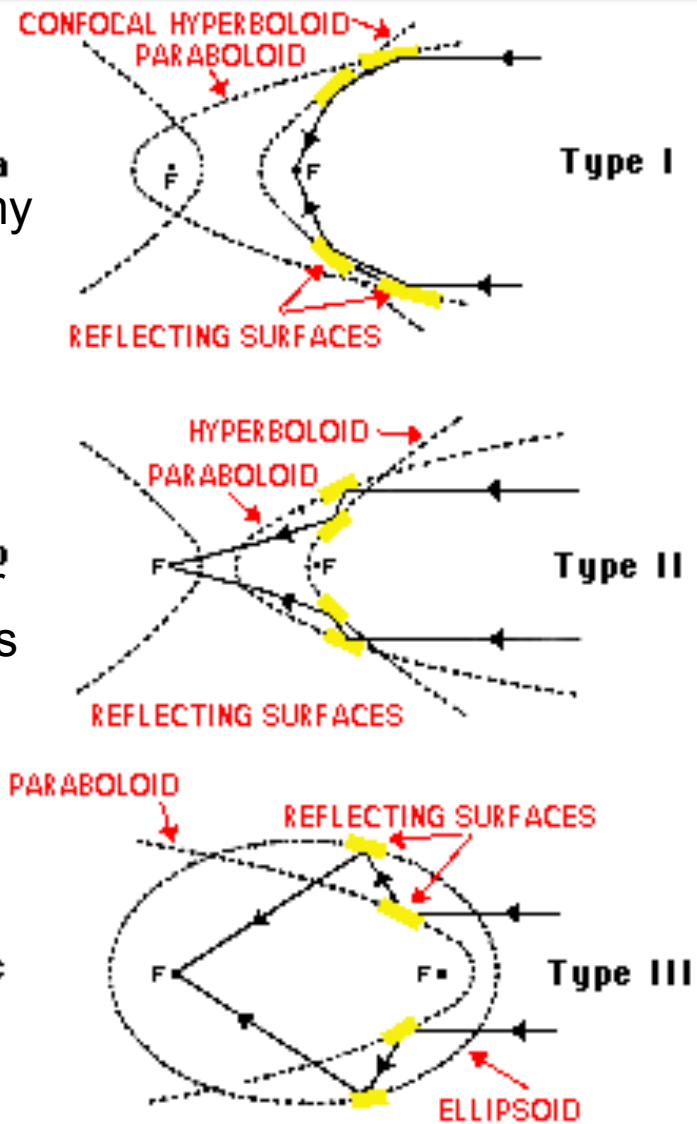


H. Wolter, Ann. Der Phys., NY10, 94 (1952)

Fine for
X-ray astronomy **a**

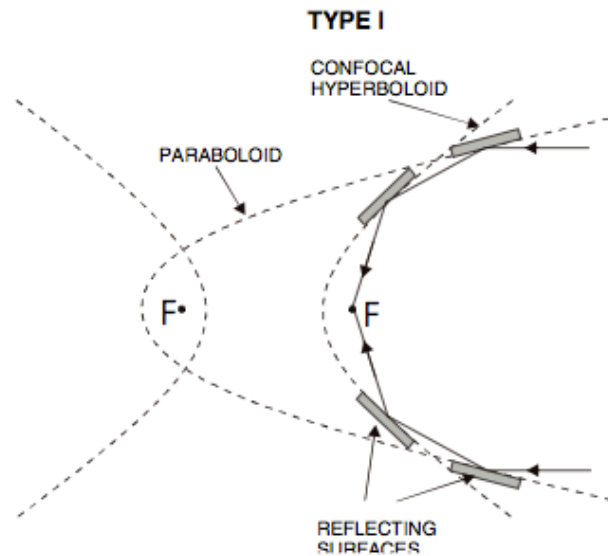
Applied in solar
X-ray telescopes **b**

Not adopted **c**

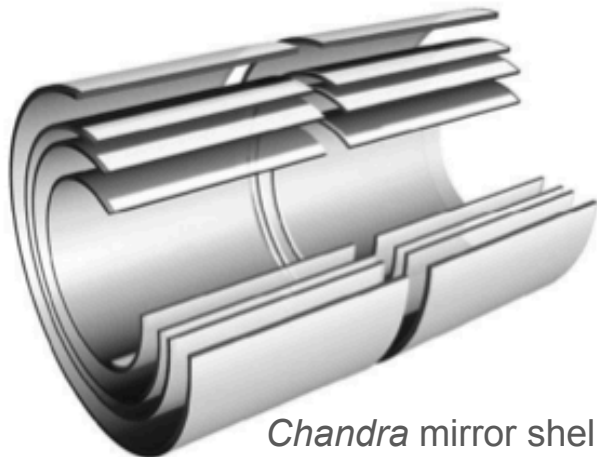


Wolter's solution: double mirror

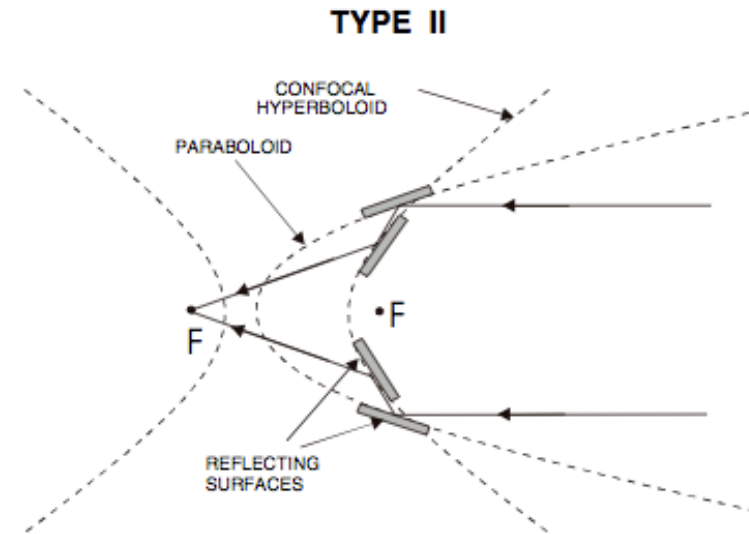
Grazing reflection and mirror shapes. VI



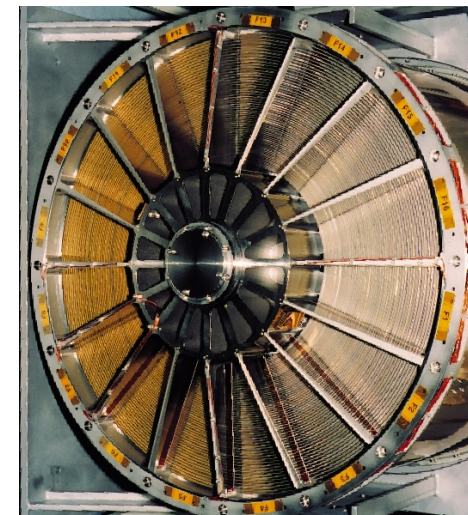
Wolter-I optics
Paraboloid → Hyperboloid



Chandra mirror shells (4)



Wolter-II optics
Paraboloid → Hyperboloid (ext. surface)

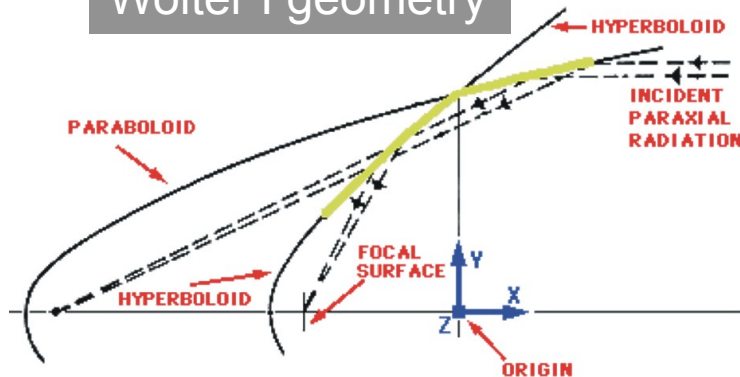


XMM-Newton
mirror shells (58)

Grazing reflection and mirror shapes. VII

WOLTER I geometry

Wolter I geometry



- guarantees the minimum focal length for a given aperture
- allows us to nest together many co-focal mirror shells

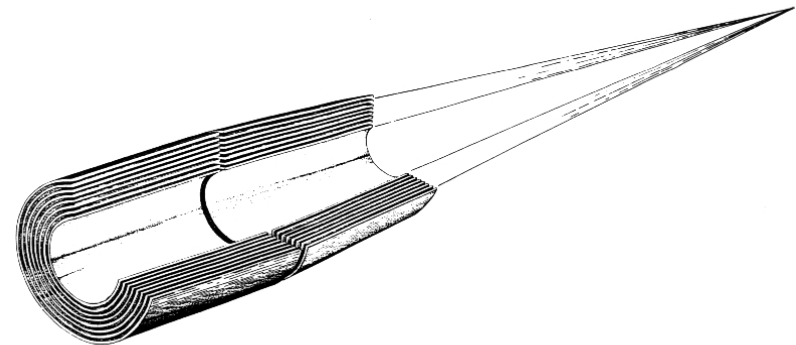
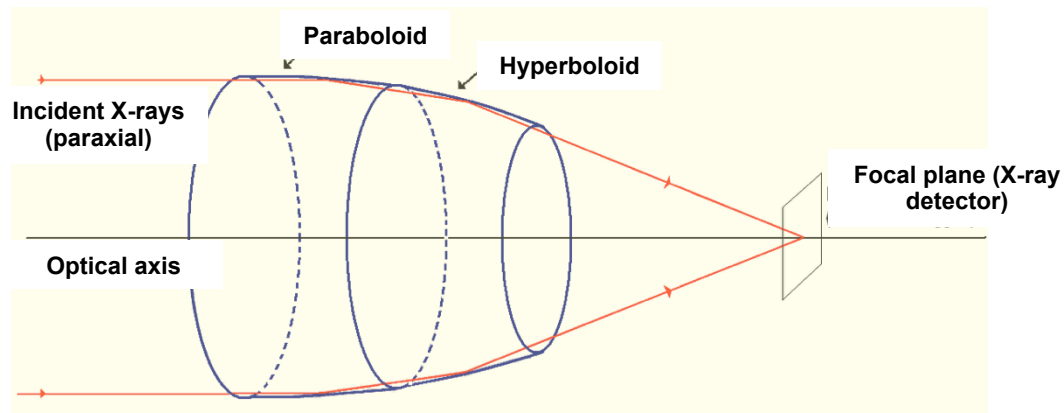
$$A_{\text{eff}} \approx F^2 \times \theta_C^2 \times R^2$$

F=focal length
 ϑ =incidence angle
 R=mirror reflectivity

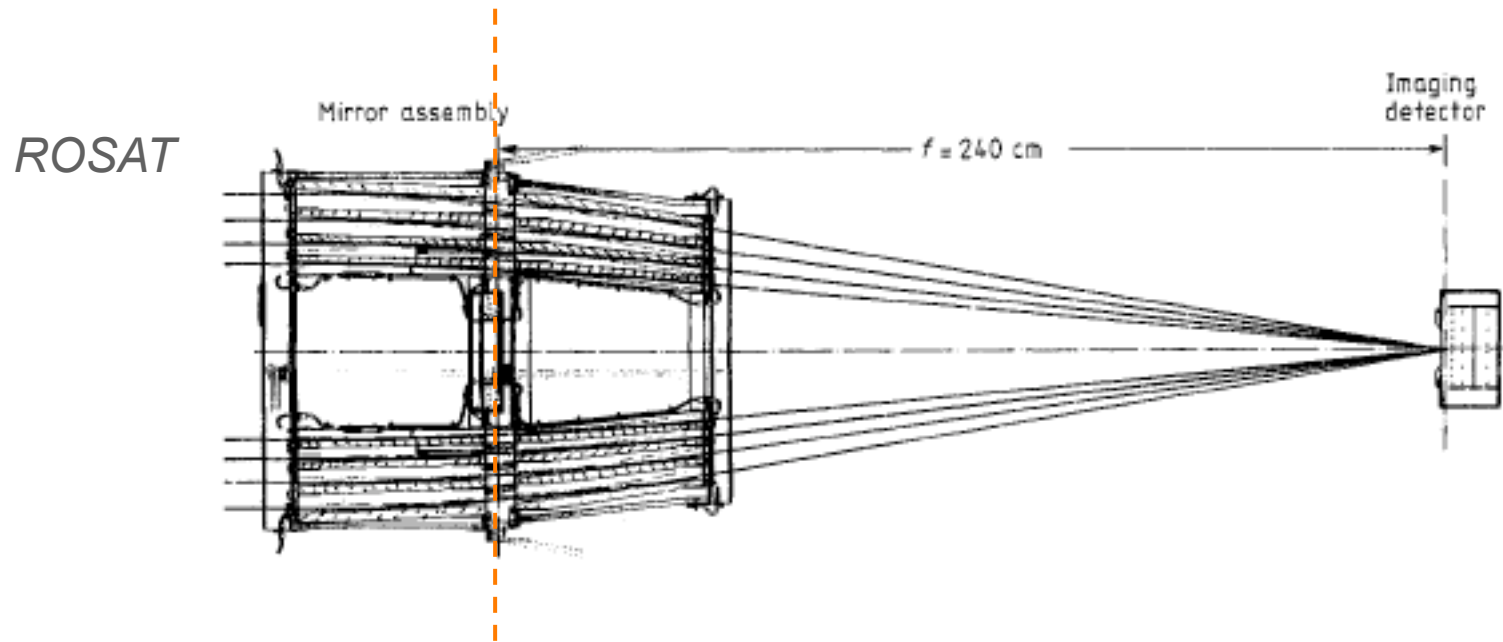
$F = R / \tan(4\theta)$: small θ , large F

$$\theta_C \propto \frac{\sqrt{\rho}}{E}$$

To increase the grazing angles, dense materials are used.
 At $E > 10$ keV, the cut-off angles for total reflection are very small also for heavy metals, hence small A_{eff} are obtained.



Grazing reflection and mirror shapes. VIII



Focal length=intersection between the paraboloid-hyperboloid surfaces and the focus

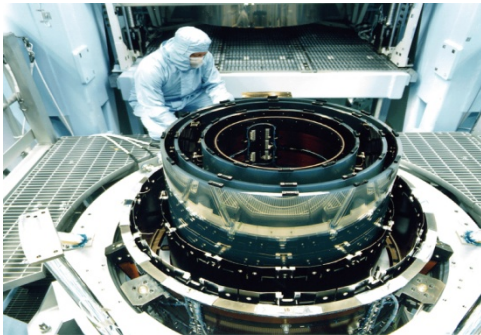
Grazing reflection and mirror shapes. IX

Alternative profiles derived from Wolter I

- Wolter-Schwarzschild profile: *it exactly satisfies the Abbe sine condition and it has been adopted for the Einstein mirrors; it is coma free but is strongly affected by spherical aberration*
- double-cone profile: *it better approximates the Wolter I at small reflection angles: it is utilized for practical reasons (- cost + effective area; soft X-ray BeppoSAX). Intrinsic on-axis focal blurring given by: $HEW \approx R/F^2$*
- polynomial profile: *parameters have been specifically optimized to maintain the same HEW in a wide field of view*
(introducing small aberration on-axis, the off-axis imaging behavior is improved
→ same principle of the Ritchey-Chretien normal-incidence telescope in the optical band)

Proposed NASA MIDEX 2020 STAR-X (following WFXT) configuration (ideal for X-ray surveys, similar PSF , 5" HPD, for the whole field of view, 1 deg²)

Mirror manufacturing techniques



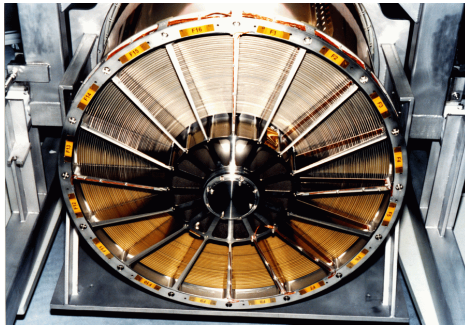
Credits: NASA

1. Classical precision optical polishing and grinding

Projects: *Einstein, Rosat, Chandra*

Advantages: *superb angular resolution*

Drawbacks: *high mirror walls → small number of nested mirror shells, high mass, high cost process*



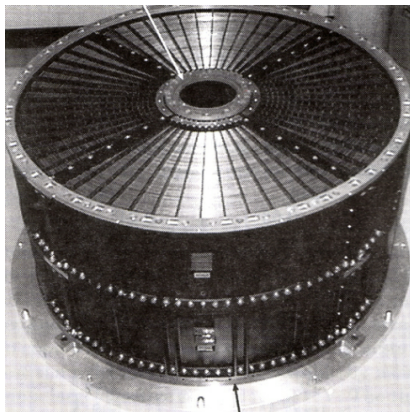
Credits: ESA

2. Replication

Projects: *EXOSAT, SAX, JET-X/Swift, XMM, ...*

Advantages: *good angular resolution, high mirror 'nesting' the same mandrels for many modules*

Drawbacks: *relatively high cost process; high mass/geometrical area ratio (if Ni is used)*



Credits: ISAS

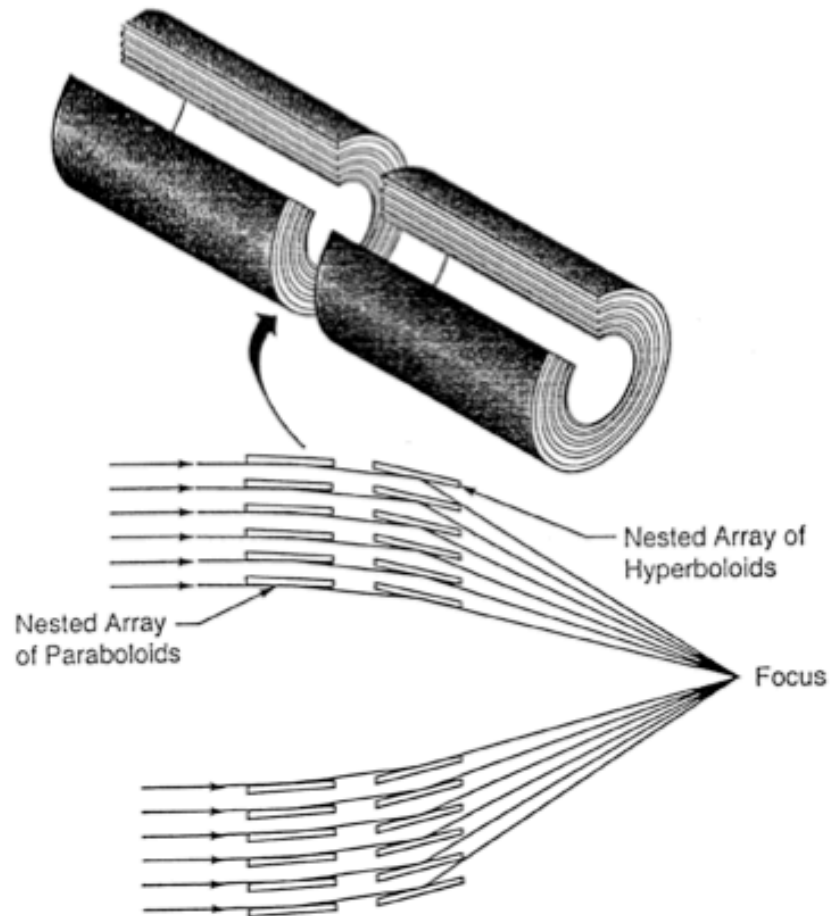
3. Thin foil mirrors

Projects: *BBXRT, ASCA, SODART, ASTRO-E*

Advantages: *high mirror "nesting" possibility, low mass/geom. area ratio (the foils are made of Al), cheap process*

Drawbacks: *until now low imaging resolutions (1-3 arcmin)*

Wolter telescopes



mission launch	no mirr.	geom area [cm ²]	graz. angles [arcmin]	highest energy [keV]
-------------------	-------------	------------------------------------	-----------------------------	----------------------------

"traditional" grazing inc. optics (e.g Zerodur)

Einstein '78	4	412	40-70	5
Rosat '90	4	1140	83-135	2
Chandra '99	4	1100	27-51	10

replicated optics

Exosat	2	80	90-110	2
Sax*	4*30	176		
Newton '99	58	6000	18-40	10

foil optics

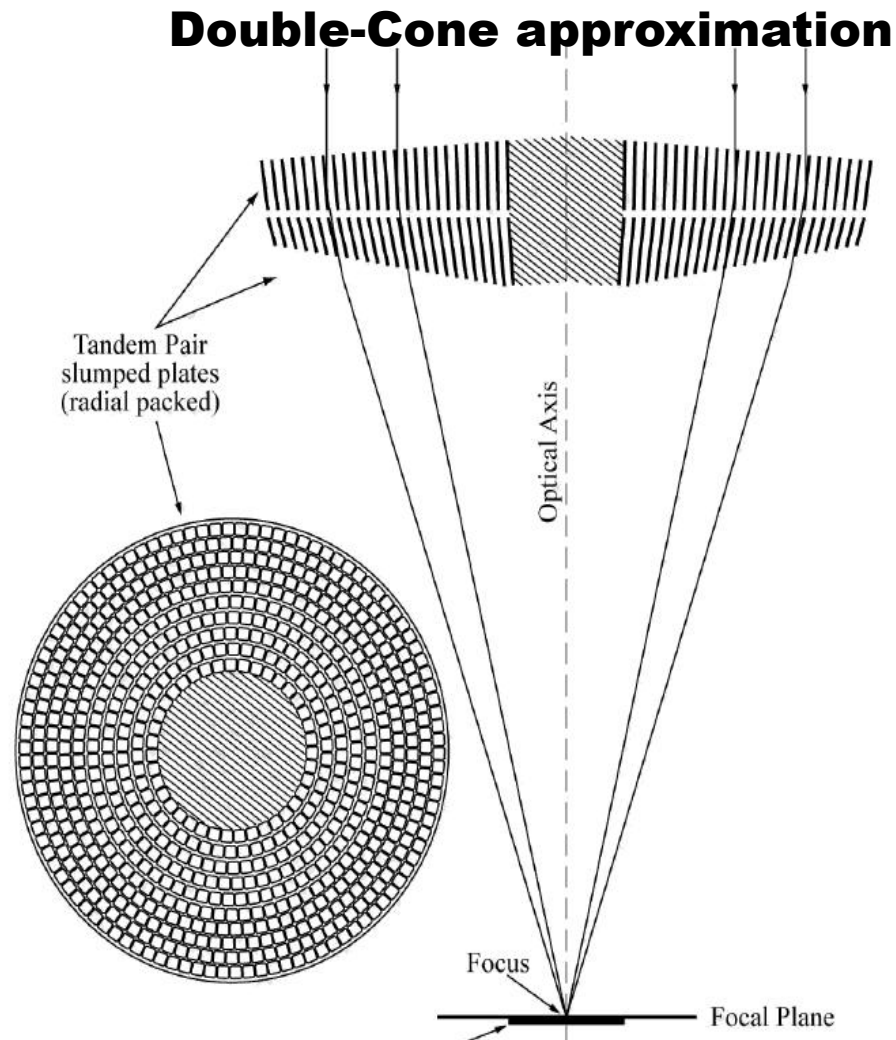
Asca*	120	4*558	21-45	12
Suzaku/XRT	175	4*873		12

*2 conic sections=approx. Wolter I optic (small θ)

multiple reflection optics (4 or more)

The future of grazing reflection

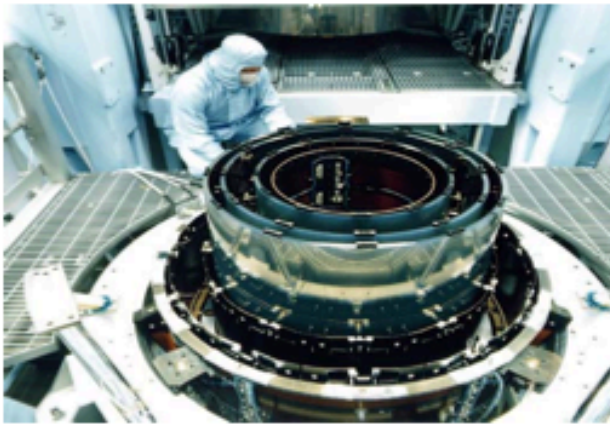
X-ray pore optics system. I



N.B.:concept introduced by D. Willingale et al, Capri 1994

X-ray pore optics system. II

Comparison with 'classical' optics

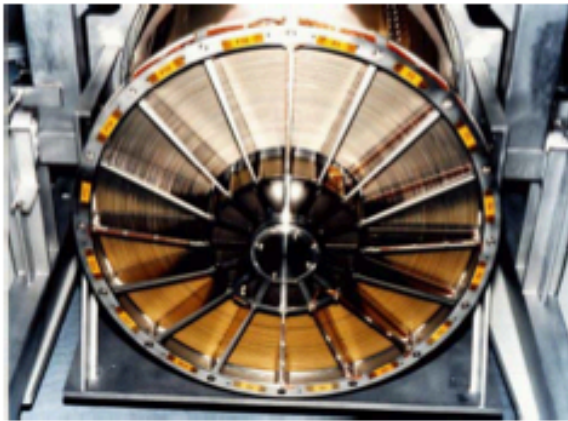


CHANDRA

0.5"

18500 kg/m²

A_{eff} @ 1 keV

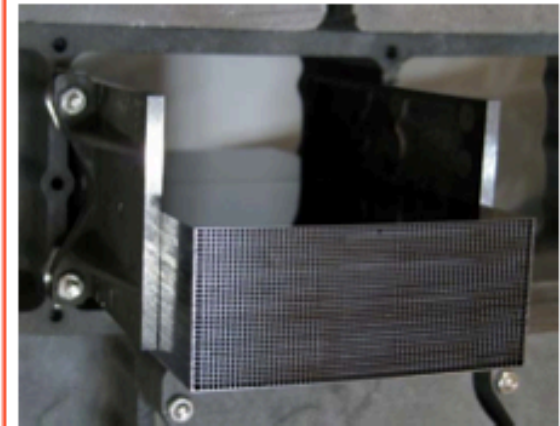


XMM-NEWTON

14"

2300 kg/m²

A_{eff} @ 1 keV



Si pore optics

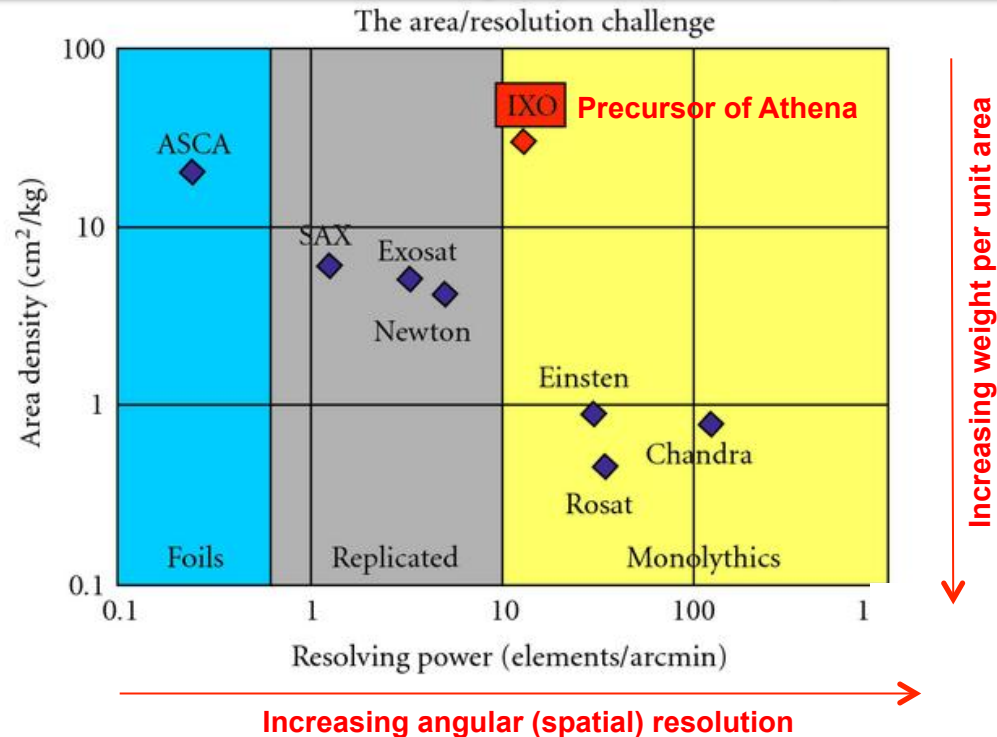
5"

200 kg/m²

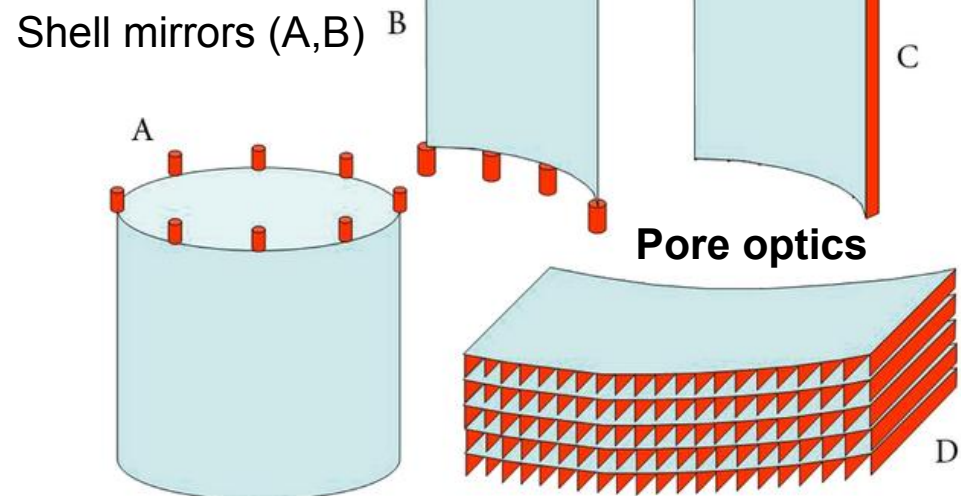
A_{eff} @ 1 keV

Athena
(~2030 mission)

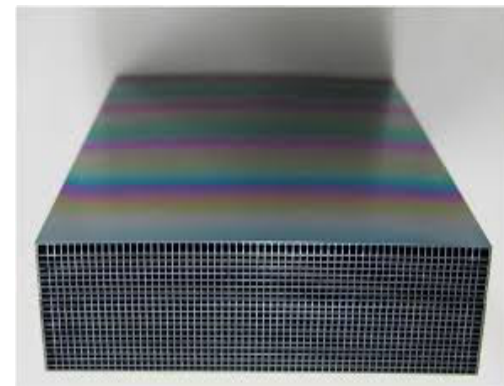
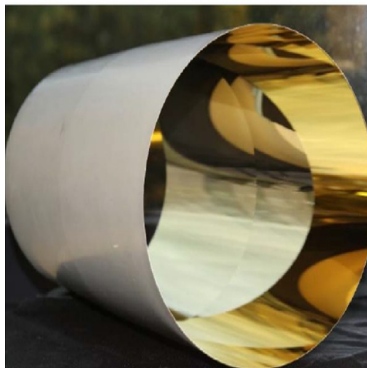
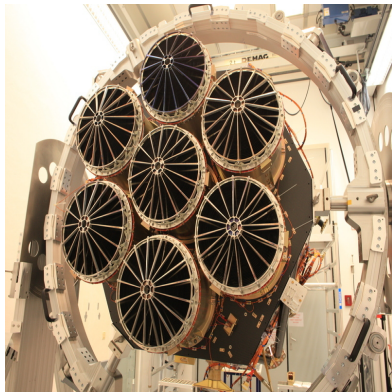
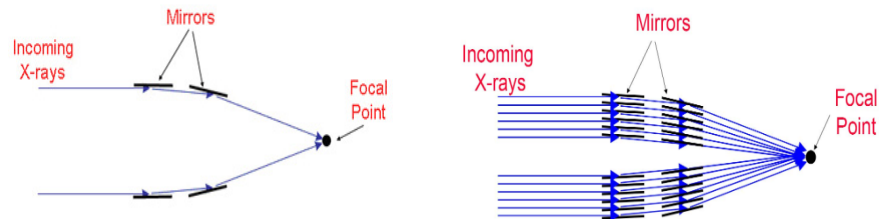
X-ray pore optics system. III



X-ray mirror elements mounted along densely spaced lines, via ribs, which attach to the back of the mirror element. Ribs provide stiffness to the mirror element and distribute the load over a line and not a point (vs. spider of shell mirrors). The mirror element becomes much stiffer, and its figure much less distorted by the mounting elements.



X-ray pore optics system. IV

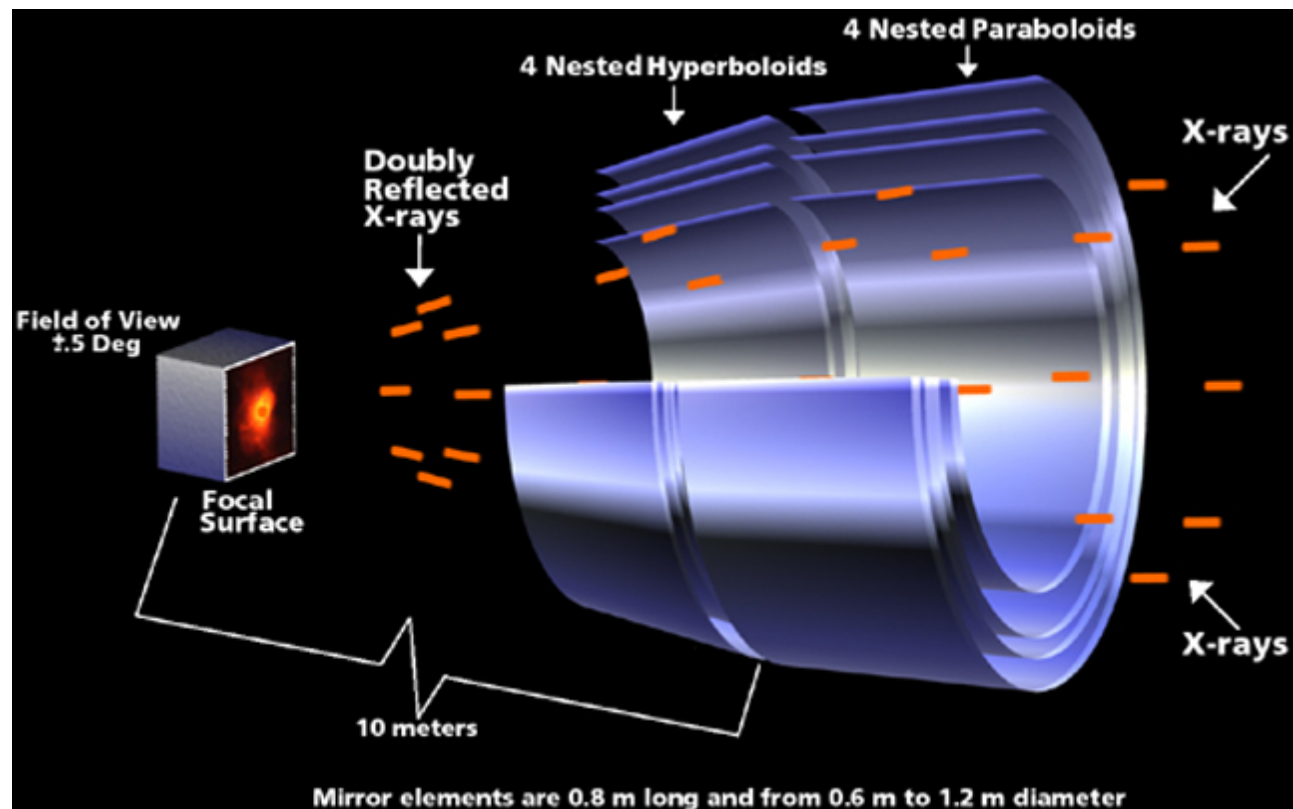


Same principle of traditional optics: the grazing incidence. About 5-10 times lighter
The question is: how to measure the effective area? Proper calibration facilities are needed

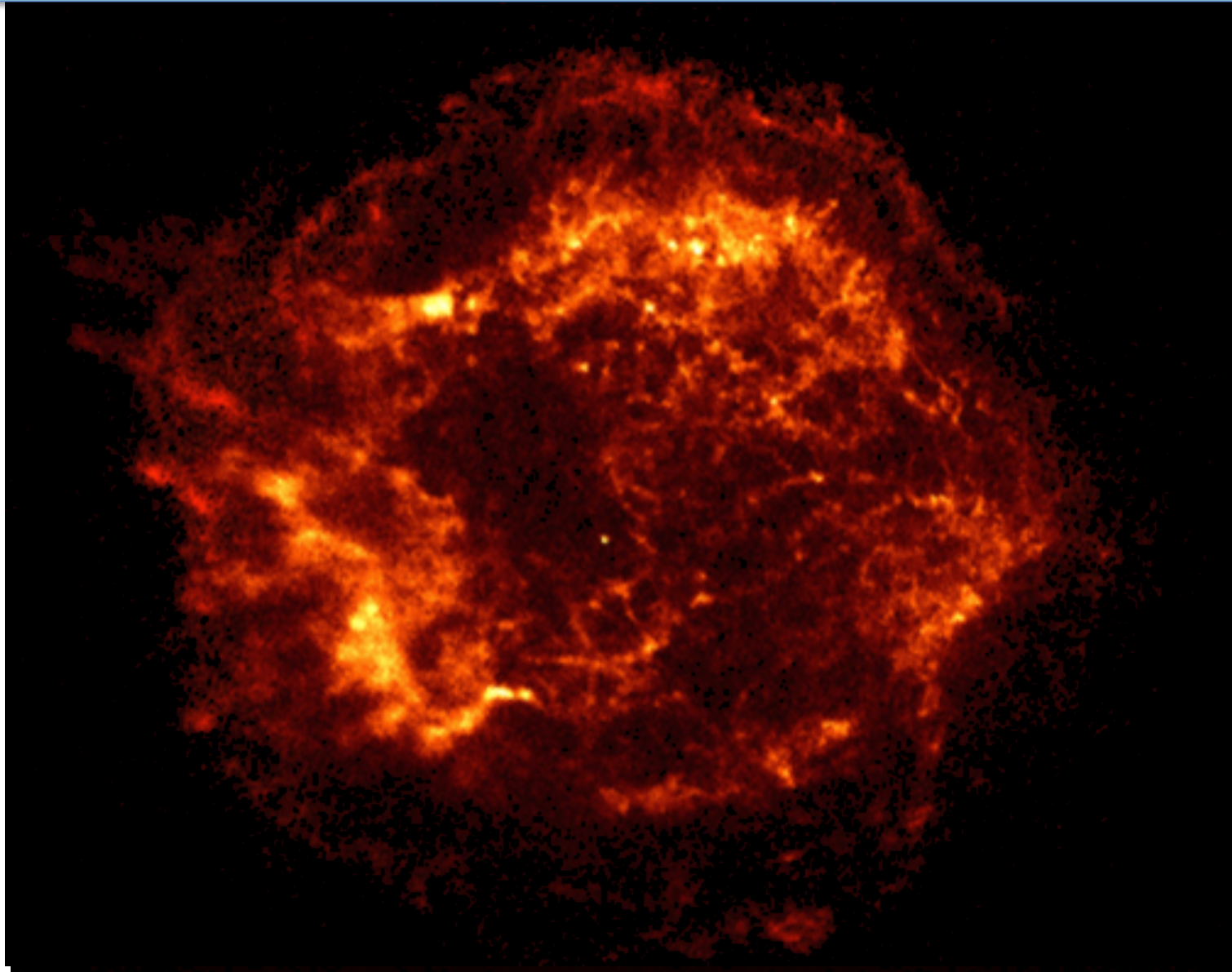
The present of grazing reflection:
some pills

Chandra

- Focal length = 10 m
- 1 module, 4 shells
- Coating = Iridium
- Angular Resolution = 0.5 arcsec HPD



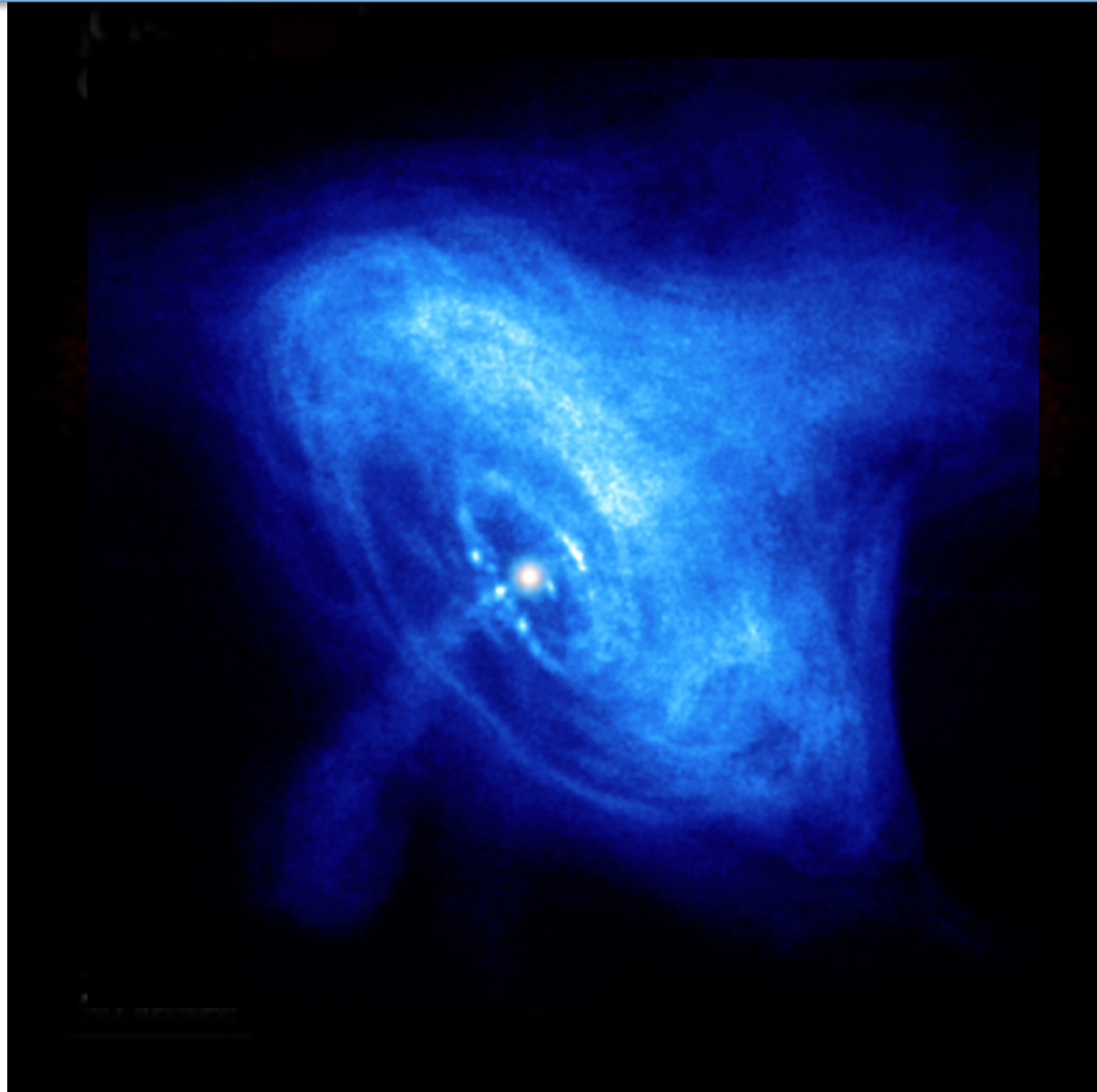
The power of spatial resolution: Cassiopeia A: *ROSAT* vs. *Chandra*



ROSAT / CXC

The power of spatial resolution:

Crab Nebula : *ROSAT* vs. *Chandra*




XMM-Newton

- Focal length = 7.5 m
- 3 modules, 58 shells/module
- Coating = Gold
- Angular Resolution = 15 arcsec HEW



XMM-Newton mirrors during integration

Image courtesy of Dornier Satellitensysteme GmbH

European Space Agency 

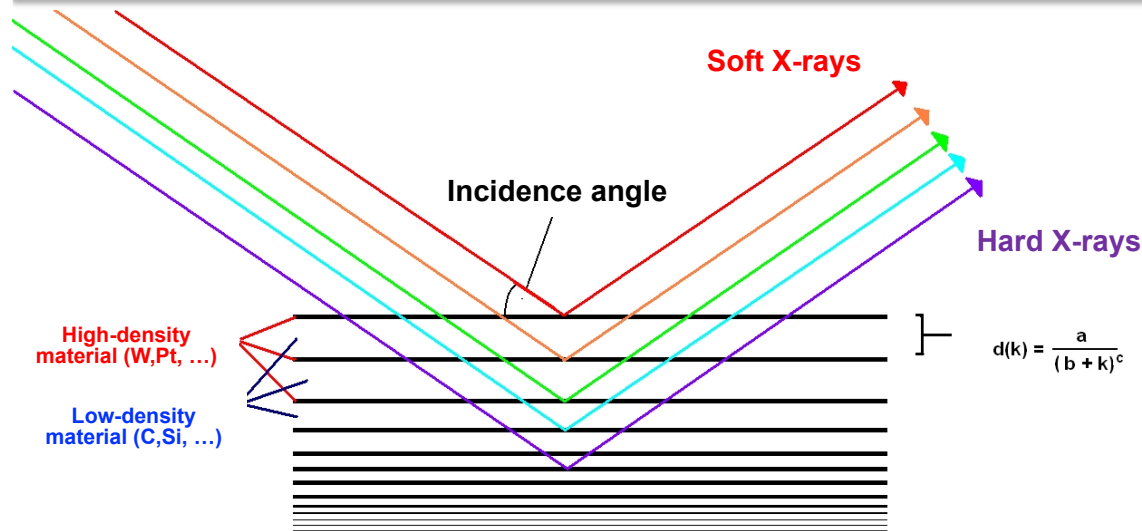
Summary of focusing (Wolter-I) telescopes

Mission	Year of launch	Upper energy limit (keV)	Focal length (m)	Mirror modules	Degree of nesting	Effective area @ 1 keV (cm ²)	On-axis resolution (HPD)
S-054/Skylab	1973	4	2.13	1	2	15	48''
S-056/Skylab	1973	1.3	1.90	1	1	9	3''
Einstein (HEAO-2)	1978	4	3.44	1	4	100	4''
EXOSAT	1983	2.5	1.09	2	2	70	24''
ROSAT	1990	2.5	2.40	1	4	420	3''
BBXRT	1990	12	3.77	2	118	450	5''
Yohkoh SXT	1991	4.0	1.54	1	1	23	<5''
ASCA (Astro-D)	1993	10	3.50	4	120	1 200	180''
Soho CDS	1995	0.5	2.58	1	1	23	<5''
BeppoSAX	1996	10	1.85	4	30	344	60''
ABRIXAS	1999	10	1.60	7	27	560	25''
Chandra (AXAF)	1999	10	10.00	1	4	780	<1''
XMM-Newton	1999	15	7.50	3	58	4 260	16''
Swift	2004	10	3.50	1	12	130	18''
Suzaku (Astro-E2)	2005						
XRT-I		12	4.75	4	175	2250	120''
XRT-S		12	4.50	1	168	2250	120''

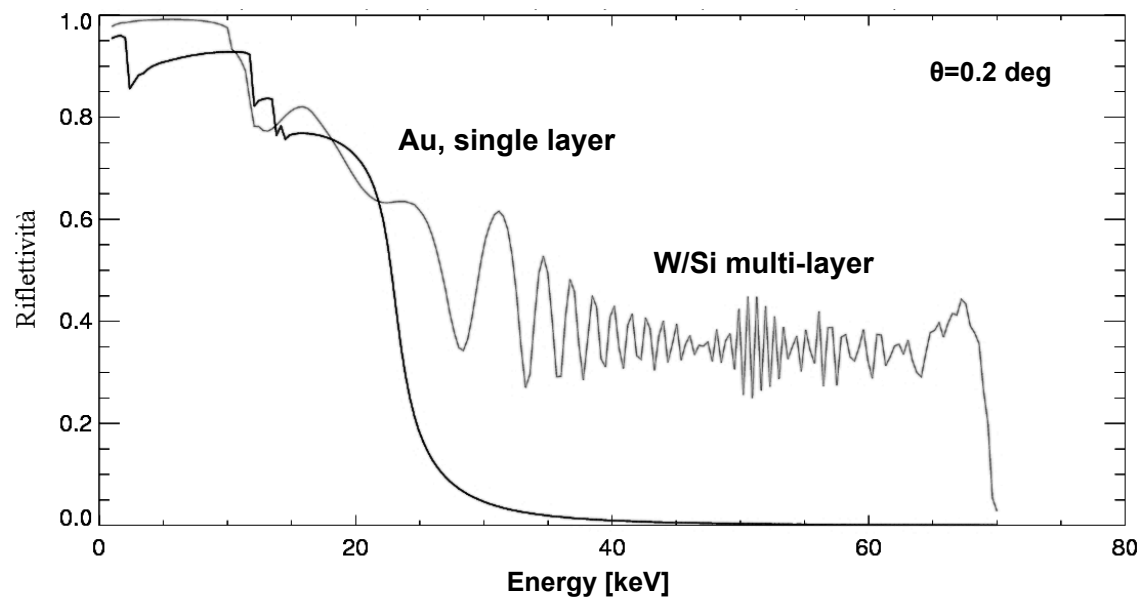
Depending on the scientific goals, each mission is a trade-off between effective area and on-axis resolution

Supermirrors multilayer coatings:
extending the energy range of X-ray telescopes

Multi-layers for hard ($E > 10$ keV) astronomy.I



Critical angles can go up to 0.2–0.4 deg



Multilayer coatings allow high reflectance beyond the critical angle by **constructive interference** of rays reflected at properly spaced Pt/C or W/Si bi-layers (200 bilayers, $60\text{\AA} \times 200 = 1\text{ micron}$)

If the d-spacing is changed in continuous way along the sequence, and the photoelectric absorption is not too large, it is possible to get reflection windows 3-4 times larger than in total reflection regime

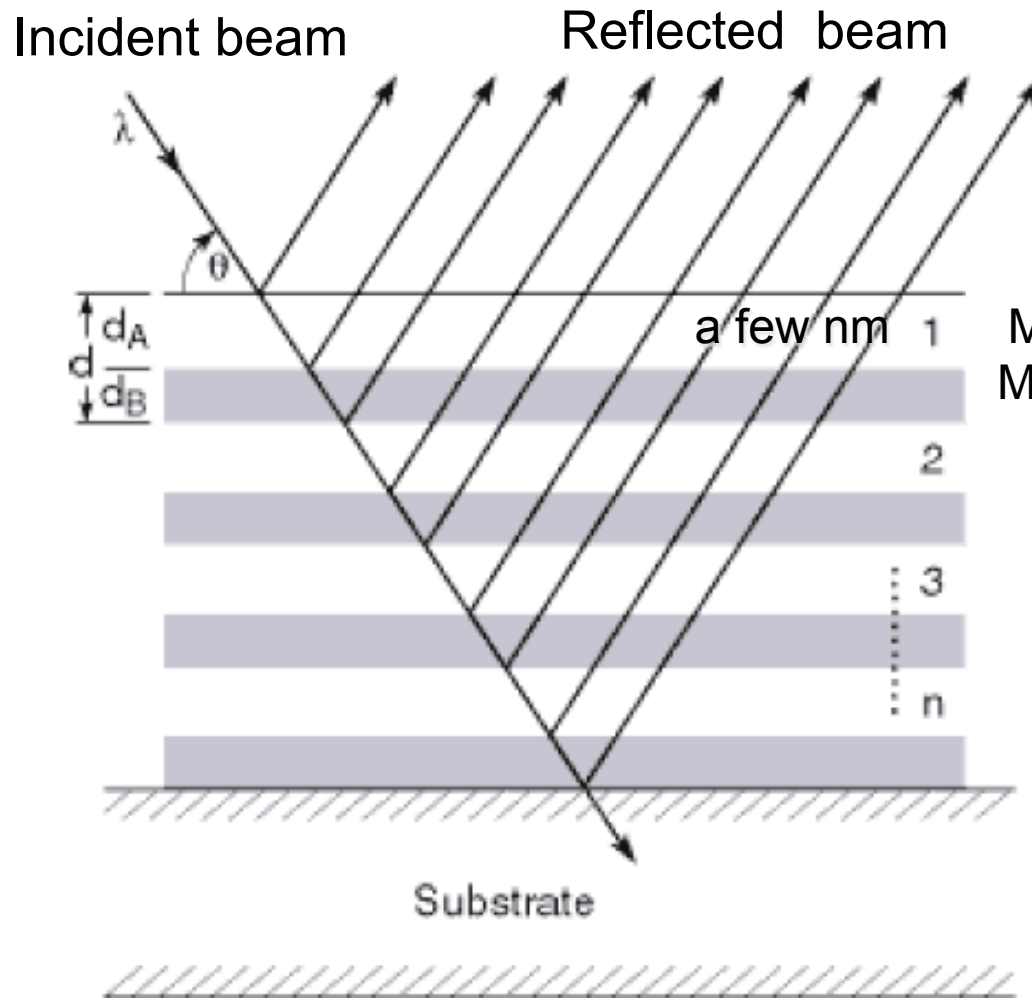
The optimal distribution of layer spacing follows in general a power law (a, b, c are parameters that should be optimized):

$$d(i) = a / (b + i)^c$$

i = bilayer index

$$a \approx \lambda / (2 \sin \theta_{inc}) \quad c \approx 0.25 \quad b > -1$$

Multi-layers for hard ($E > 10$ keV) astronomy.II



At each transition from one material to another, partial reflection occurs
→ constructive interference

Material A (Platinum, Tungsten)
Material B (Silicium, Carbonium)

This has been realized with alternate layers of high Z material, to provide a high electron density for reflection, and low Z material, to provide a phase shift with minimal absorption.

Multi-layer reflection ('supermirrors')